

The GALAH Survey and Symbiotic Stars. I. Discovery and follow-up of 33 candidate accreting-only systems

U. Munari,¹★ G. Traven,² N. Masetti,^{3,4} P. Valisa,⁵ G.-L. Righetti,⁵ F.-J. Hamsch,⁵
 A. Frigo,⁵ K. Čotar,⁶ G. M. De Silva,^{7,8} K. C. Freeman,⁹ G. F. Lewis,¹⁰ S. L. Martell,^{11,12}
 S. Sharma,^{10,12} J. D. Simpson,^{11,12} Y.-S. Ting,¹³ R. A. Wittenmyer¹⁴ D. B. Zucker,^{8,12,15}

¹INAF Astronomical Observatory of Padova, 36012 Asiago (VI), Italy

²Lund Observatory, Department of Astronomy and Theoretical Physics, Box 43, SE-221 00 Lund, Sweden

³INAF Osservatorio di Astrofisica e Scienza dello Spazio, via Gobetti 93/3, 40129 Bologna, Italy

⁴Departamento de Ciencias Físicas, Universidad Andrés Bello, Fernández Concha 700, Las Condes, Santiago, Chile

⁵ANS Collaboration, c/o Astronomical Observatory, 36012 Asiago (VI), Italy

⁶Faculty of Mathematics and Physics, University of Ljubljana, Jadranska 19, 1000 Ljubljana, Slovenia

⁷Australian Astronomical Optics, Macquarie University 105 Delhi Rd, North Ryde, NSW 2113, Australia

⁸Macquarie University Research Centre for Astronomy, Astrophysics & Astrophotonics, Sydney, NSW 2109, Australia

⁹Research School of Astronomy & Astrophysics, Australian National University, ACT 2611, Australia

¹⁰Sydney Institute for Astronomy, School of Physics, A28, The University of Sydney, NSW 2006, Australia

¹¹School of Physics, UNSW, Sydney, NSW 2052, Australia

¹²Centre of Excellence for Astrophysics in Three Dimensions (ASTRO-3D), Australia

¹³Department of Astrophysical Sciences, Princeton University, Princeton, NJ 08544, USA

¹⁴University of Southern Queensland, Centre for Astrophysics, USQ Toowoomba, QLD 4350 Australia

¹⁵Department of Physics and Astronomy, Macquarie University, Sydney, NSW 2109, Australia

Accepted XXX. Received YYY; in original form ZZZ

ABSTRACT

We have identified a first group of 33 new candidates for symbiotic stars (SySt) of the accreting-only variety among the 600 255 stars so far observed by the GALAH high-resolution spectroscopic survey of the Southern Hemisphere, more than doubling the number of those previously known. GALAH aims to high latitudes and this offers the possibility to sound the Galaxy for new SySt away from the usual Plane and Bulge hunting regions. In this paper we focus on SySt of the M spectral type, showing an H α emission with a peak in excess of 0.5 above the adjacent continuum level, and not affected by coherent radial pulsations. These constraints will be relaxed in future studies. The 33 new candidate SySt were subjected to a vast array of follow-up confirmatory observations (X-ray/UV observations with the *Swift* satellite, search for optical flickering, presence of a near-UV upturn in ground-based photometric and spectroscopic data, radial velocity changes suggestive of orbital motion, variability of the emission line profiles). According to Gaia *e*DR3 parallaxes, the new SySt are located at the tip of the Giant Branch, sharing the same distribution in $M(K_S)$ of the well established SySt. The accretion luminosities of the new SySt are in the range 1–10 L_\odot , corresponding to mass-accretion rates of 0.1–1 $10^{-9} M_\odot \text{ yr}^{-1}$ for WDs of 1 M_\odot . The M giant of one of the new SySt presents a large Lithium over-abundance.

Key words: binaries: symbiotic stars – methods: data analysis – Galaxy: stellar content

1 INTRODUCTION

Symbiotic stars (SySt) are interacting binaries where a red giant (RG) fuels a white dwarf (WD) or a neutron star (NS) companion via accretion (either through Roche-lobe overflow or wind intercept). Systems harboring NSs are a recent addition to

this class of celestial objects (Masetti et al. 2006, 2007a,b, 2011; Bozzo et al. 2018; Yungelson, Kuranov, & Postnov 2019) and constitute a few percent of the known total (Merc, Gális, & Wolf 2019a), the vast majority containing WDs (Mukai et al. 2016; Sokolowski et al. 2017; Akras et al. 2019). For some time, a main sequence star accreting from the RG at very high rates (10^{-6} to $10^{-4} M_\odot \text{ yr}^{-1}$) was considered a viable scenario for SySt in general (Kenyon & Webbink 1984), but this has been pro-

★ E-mail: ulisse.munari@inaf.it

gressively abandoned in the light of expanding observational data, especially in the far UV and X-rays (Sokoloski et al. 2006; Skopal et al. 2006; Mohamed & Podsiadlowski 2012; Luna et al. 2013; Skopal & Cariková 2015; Lutovinov et al. 2020). Even if we will focus on RG+WD systems, the results of this paper are independent on the actual nature of the accreting star.

The RG+WD symbiotic stars are broadly divided into two major groups (see the recent review by Munari et al. 2019 for details): those *accreting-only* (*acc*-SySt) whose optical spectra are dominated by the RG with no or weak emission lines, and the *burning-type* (*burn*-SySt) displaying a strong nebular continuum and a rich emission line spectrum: they originate from the wind of the RG, which is largely ionized by the very hot and luminous WD undergoing surface nuclear burning of accreted material.

SySt are believed to spend most of their time in the accreting-only phase, quietly accumulating material on the surface of the WD. When enough has been piled up, nuclear burning ignites. If the accreted matter is electron degenerate, the burning proceeds explosively. It quickly reaches the Fermi temperature (a matter of minutes, Starrfield et al. 2008) and ejects most of the accreted envelope at high velocity (thousands of km s⁻¹). Radio-interferometry has nicely resolved the expansion of ejecta following, for ex., the 2006 outburst of RS Oph (O’Brien et al. 2006) and that of 2010 for V407 Cyg (Giroletti et al. 2020), the latter being also the first nova event ever detected in GeV γ -rays by the Fermi satellite (Cheung et al. 2010). The resulting nova outburst can repeat on time-scales as short as years/decades if the WD mass is close to the Chandrasekhar limit, like in the case for T CrB, RS Oph, V407 Cyg or V3890 Sgr. If the matter accreted on the WD is instead not electron-degenerate, the nuclear burning proceeds in thermal equilibrium, and no mass is ejected. The event takes a few years to reach peak brightness (Fujimoto 1982), and requires many decades to a few centuries to burn the accreted envelope and let the system return to low luminosity. Some of the best examples of this type are AG Peg, HM Sge, V1016 Cyg and V4368 Sgr.

There is a clear disproportion among catalogued SySt in favor of the *burn*-SySt type, and the known examples of the *acc*-SySt variety are believed to be just the tip of the iceberg (Mukai et al. 2016, hereafter Mk16). Between 15 and 20 are currently known of the *acc*-SySt type. Symbiotic stars were originally proposed by Munari & Renzini (1992) as possible progenitors of type Ia supernovae, and the viability of this single-degenerate channel obviously relies on the total number of SySt spread throughout the Galaxy, which in turn heavily depends on the number of *acc*-SySt. The latter have been usually discovered as counterparts of satellite UV/X-ray sources, while the *burn*-SySt can be easily spotted at optical wavelengths through the whole Galaxy and the Local Group thanks to their outstanding emission-line spectrum (with ionization up to [FeX] and beyond).

The subtle way the optically-quiet *acc*-SySt have been usually discovered is well epitomized by SU Lyn, a $V \sim 8$ mag, M6III giant at 650 ± 35 pc distance (Gaia Collaboration et al. 2018). For decades it was a completely unnoticed field star, with just an old report about semi-regular photometric variability which granted it a variable star name (Kippenhahn 1955). While looking for optical counterparts of hard X-ray sources newly discovered by the *Swift* satellite, it was noted that SU Lyn lay within the error box of one of them: 4PBC J0642.9+5528. Follow-up observations were organized with *Swift* (to refine the position and the properties of the X-ray source) and with Asiago telescopes to investigate if the optical spectra of SU Lyn could betray peculiarities supporting a physical association with the *Swift* hard X-ray source. The association was proved by a

large flux excess observed at bluest optical wavelengths ($\lambda \leq 4000$ Å) and by the presence on high-resolution spectra of weak and variable emission in H α and [NeIII] lines (cf. Mk16).

The limited sensitivity of current X-ray satellites (soon to change thanks to *e*-ROSITA sky survey, Merloni et al. 2012) restricts the serendipitous discovery of *acc*-SySt to those that lie within ~ 1 kpc from the Sun, implying that many of their red giants rank among naked-eye objects (like 4 Dra, HR 1105 or *o* Cet). To sample a much larger fraction of the RG in our Galaxy, we have devised a reverse strategy, and first exploratory results are presented in this paper: digging through large spectroscopic surveys in search for the signatures of accretion onto a companion to the RG, primarily the presence of Balmer emission lines having a flux and a profile compatible with an origin in an accretion disk around a degenerate companion. The candidate *acc*-SySt identified this way can then be subjected to follow-up confirmatory observations, including pointing with X-ray/UV satellites. The GALAH survey of the southern hemisphere (De Silva et al. 2015) offers an ideal hunting opportunity: a large number (aiming at >1 million) of randomly selected southern stars in the $12 \leq V_{JK} \leq 14$ mag range are observed at high S/N and high spectral resolution with the AAT 3.9m telescope + fibre-fed spectrograph HERMES, over four distinct wavelength ranges that include H α and H β lines.

In this first paper we outline the methodologies guiding our search among GALAH spectra for candidate *acc*-SySt, report on the discovery of a first batch of 33 new candidates (about doubling the total known so far), and describe the results of a wide range of follow-up observations aiming to confirm their *acc*-SySt nature. We encourage further observations by the community in order to validate their classification.

2 THE GALAH SURVEY

2.1 Motivation

The Galactic Archaeology with HERMES (GALAH, De Silva et al. 2015) is an ongoing spectroscopic survey whose ambitious goal is to unveil the formation and history of the Milky Way. This is the focus of the field of Galactic Archaeology, which tries to determine how the fossil remnants of star-forming regions and effects of ancient mergers paint the picture of our Galaxy that we observe and measure today. This complex endeavor can be accomplished by studying the detailed chemical composition and other properties of stars in distinct regions of the Milky Way.

The Galactic archaeology community argues that the complete Galaxy formed gradually over time. This formation history can be traced back by investigating remnants of initial building blocks or subsequent additions through mergers, which have been disrupted in the course of evolution and are now dispersed around the Galaxy. The theoretical concept of chemical tagging (Freeman & Bland-Hawthorn 2002) demonstrates that individual galactic components should have preserved their original chemical signature over time. It is therefore essential to disentangle their formation site from migration history in order to explain the current mixture of stellar populations.

GALAH aims to achieve this by measuring the abundance of up to 31 chemical elements coming from seven independent major groups with different nucleosynthetic origin: light proton-capture elements Li, C, O; α -elements Mg, Si, Ca, Ti; odd-Z elements Na, Al, K; iron-peak elements Sc, V, Cr, Mn, Fe, Co, Ni, Cu, Zn; light and heavy slow neutron capture elements Rb, Sr, Y, Zr, Ba, La; and

rapid neutron capture elements Ru, Ce, Nd and Eu (De Silva et al. 2015).

2.2 Instrument

The goals of the GALAH survey were the main driver for the construction of the High Efficiency and Resolution Multi-Element Spectrograph (HERMES, Barden, et al. (2010); Sheinis et al. (2015)), a multi-fibre spectrograph working in tandem with the 3.9-metre Anglo-Australian Telescope (AAT) situated at the Siding Spring Observatory, Australia. The spectrograph has a resolving power of $R \sim 28,000$ (or $R \sim 45,000$ when slit mask is used) and records spectra in four separate wavelength ranges given in Table 1. The total spectral coverage is therefore approximately 1000 \AA , including the important diagnostic lines $H\alpha$ and $H\beta$, together with lines of numerous chemical elements that are necessary to fulfil the ambitions of the GALAH survey.

The AAT uses the Two Degree Field (2dF) robotic positioning system with two identical plates that are used to precisely position fibres at designated locations. This configuration allows HERMES to simultaneously record spectra from up to 392 fibres distributed over a 2° diameter field of the night sky, with an additional 8 fibres used for the telescope guiding. During the exposure with the first plate, the robotic positioner places fibres on the second plate, where each complete process of fibre allocation takes about half an hour per plate. HERMES can typically achieve a signal to noise ratio (SNR) ~ 100 per resolution element at magnitude $V=14$ in the red arm during a 1-hour long exposure. To achieve as high SNR as possible, minimize atmospheric diffraction, and in order not to lose light due to the fibres' field of view of only $2''$, all observations are ideally carried out close to the meridian.

2.3 Selection function

The main selection function of the GALAH survey is relatively simple: it avoids the crowded regions of the Galactic plane ($|b| > 10^\circ$), accounts for the nominal telescope operations ($-80^\circ \leq \delta \leq +10^\circ$) and restricts observations by apparent magnitude ($12 < V_{JK} < 14$), while being colour independent. There is an additional requirement for field selection: the density of stars has to be at least 400 per π square degrees to match the number of fibres and field of view of the fibre positioner. The input catalogue for observations is based on the Two Micron All-Sky Survey (2MASS Skrutskie et al. 2006), with V_{JK} approximating standard V magnitude and being computed as (for more details see Martell et al. 2017):

$$V_{JK} = K + 2(J - K + 0.14) + 0.382e^{(J-K-0.2)/0.5} \quad (1)$$

The majority of observations are performed with the above described selection function. Additionally, GALAH employs a bright mode ($9 < V_{JK} < 12$) during twilight or poor observing conditions, and a faint mode ($12 < V_{JK} < 14.5$) when fields with normal or bright configuration are not available to be observed.

The spectroscopic data used in this work is further complemented by observations of the K2-HERMES survey Wittenmyer et al. (2018) and the TESS-HERMES survey Sharma et al. (2018), which are carried out with the same observational and data reduction setup as the GALAH survey, albeit with their peculiar selection functions focusing on K2 (Howell et al. 2014) and TESS (Ricker et al. 2015) targets, respectively.

Together, the above described observations yield a dataset of

Table 1. Short and long wavelength limits (\AA) of the four spectral intervals recorded by the GALAH survey.

interval	start	end
blue	4718	4903
green	5649	5873
red	6481	6739
far red	7590	7890

625 757 successfully reduced stellar spectra, of which a small fraction belongs to repeated observations of 600 255 unique stars observed by GALAH at the time of writing of this paper. They represent dwarf as well as giant stars, the former consisting of mostly nearby stars (closer than 2 kpc) while the latter probing distances as far as the Galactic center.

2.4 Data reduction and analysis

Every stellar spectrum recorded by the HERMES spectrograph and used in this work is homogeneously reduced by an automatic reduction pipeline, thoroughly described by Kos et al. (2017). We hereby provide only a brief explanation of this reduction procedure.

The path from a 2D image recorded in each of the HERMES arms to a one-dimensional, continuum-normalized and zero-RV-shifted spectrum starts with the following steps: raw image cosmetic corrections, spectral tracing, optical aberrations correction, scattered light and apertures cross-talk removal, wavelength calibration, sky subtraction, and telluric absorption removal. Afterwards, spectra are continuum-normalized and shifted into their rest-frame by cross-correlating them with a set of 15 AMBRE model spectra (de Laverny et al. 2012). This procedure also yields initial radial velocities, while initial stellar parameters (T_{eff} , $\log g$, $[\text{Fe}/\text{H}]$) are determined by a (larger) grid of 16 783 AMBRE spectra. These, internally also called GUESS parameters, were reported in the first GALAH data release (Martell et al. 2017). The spectra are then directed to the analysis pipeline with the aim of delivering precise and accurate stellar atmospheric parameters and individual elemental abundances, which constitute the core of results reported in subsequent GALAH data releases.

2.5 The new SySt probed by GALAH

Most of the known SySt have been discovered during photographic objective-prism surveys of the Galactic plane and Bulge (e.g. Merrill & Burwell 1950; Sanduleak & Stephenson 1973; Henize 1976), many of which were initially classified and studied as planetary nebulae. Their true nature was generally unveiled by infrared observations catching the presence of a cool giant in the system (Allen 1982, 1984; Sabbadin, Falomo, & Ortolani 1987). The same objective-prism technique was applied also to the Magellanic Clouds and several SySt were discovered there too (Walker 1983; Morgan 1992). Searches for SySt in external galaxies has steadily progressed over the years (Angeloni et al. 2014; Gonçalves et al. 2008, 2012, 2015; Mikołajewska, Caldwell, & Shara 2014; Mikołajewska et al. 2017; Roth et al. 2018; Kniazev et al. 2009; Drozd et al. 2019), and the current total of known extra-galactic SySt amounts to ~ 70 systems (Akras et al. 2019; Chen, Liu, & Shan 2019; Merc, Gális, & Wolf 2019b). New surveys aiming to SySt within the Local Group

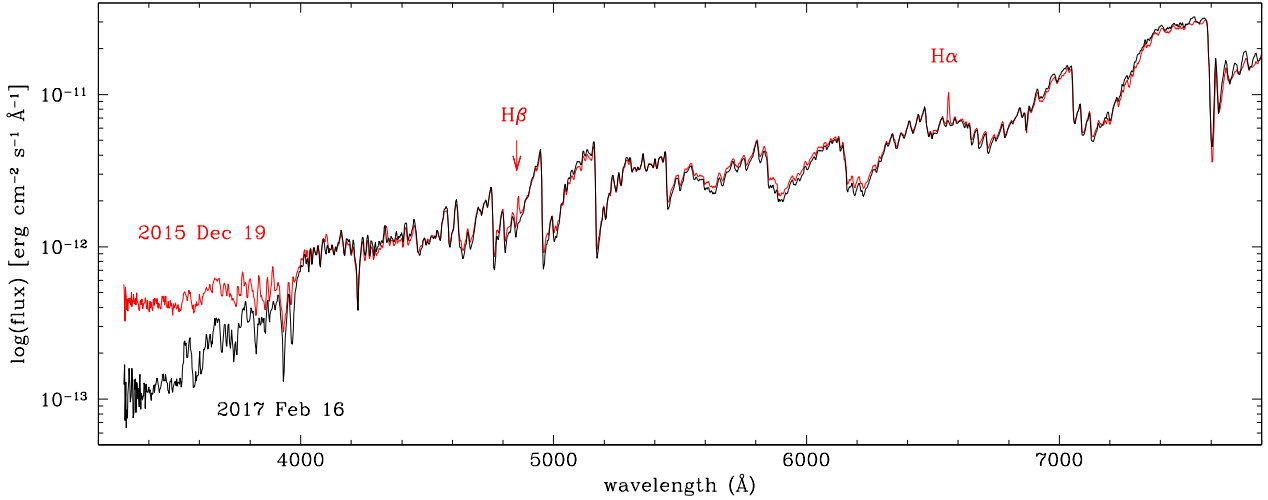


Figure 1. Two spectra of SU Lyn, a prototype of the accreting-only symbiotic stars, to illustrate the differences between low (black) and high (red) accretion rates (Asiago 1.22m telescope). A higher rate causes a brightening of the accretion disk around the white dwarf, which manifests as an excess near-UV brightness ($\lambda \leq 4000 \text{ \AA}$) and detectable emission lines (primarily hydrogen Balmer lines).

(Angeloni et al. 2019) promise to increase such numbers, especially for the *burn*-SySt type.

Systematic searches for new SySt have also been performed in recent years through our Galaxy. The IPHAS survey (Drew et al. 2005) targeted the plane of the Milky Way for emission-line objects, among which many new candidate SySt were identified by Corradi et al. (2008, 2010, 2011) and Rodríguez-Flores et al. (2014). SySt were also hunted toward the Bulge by Miszalski, Mikołajewska, & Udalski (2013) and Miszalski & Mikołajewska (2014). The current total of confirmed Galactic SySt is about 250 (Akras et al. 2019; Merc, Gális, & Wolf 2019b).

No recent survey has extensively probed the Galaxy for SySt toward directions other than low on the Plane or toward the Bulge. This is a gap we intend to fill with the help of the GALAH survey, that is exploring the Galaxy primarily at high latitudes. In this way a more complete census of SySt will be possible toward all stellar populations, allowing a more informed comparison with the predictions about the total number of SySt spread throughout the Galaxy. Such estimates vary over a wide range: from 1,200–15,000 of Lü, Yungelson, & Han (2006), or 3,000–30,000 of Yungelson et al. (1995) and Zhu et al. (2010), to 3,000 of Allen (1984), 30,000 of Kenyon et al. (1993), and 300,000 of Munari & Renzini (1992). The large spread is in part accounted for by differences in the adopted binary evolution codes and stellar population synthesis, or by the type of SySt considered (burning or accreting only), and also by the ratio between SySt currently in an active state (and therefore detectable to observations) and those dormant (and indistinguishable from single, field cool giants). The populations of SySt containing a NS is generally estimated at 100–1,000 (eg. Lü et al. 2012), or about 1% of those harboring a WD.

3 SU LYNCIS, A PATH-FINDER

As remarked earlier, several *acc*-SySt have been known for quite a while. A few of them present emission lines bright enough to be recognizable even on objective prism plates or low resolution optical spectra. They are well epitomized by EG And, an M2III

giant orbited every 481 days by a WD, whose accretion luminosity is a few $10^2 L_{\odot}$ (Nuñez et al. 2016).

The discovery of SU Lyn by Mk16 revealed a “*hidden and potentially large population*” of *acc*-SySt accreting at much lower rates, with accretion luminosities a couple of orders of magnitude lower than in EG And, and therefore not detectable by conventional observations at optical wavelengths. This paper aims to specifically discover more of these SySt characterized by low accretion luminosities ($L_{\text{acc}} \sim 1\text{--}10 L_{\odot}$). As the properties of SU Lyn will guide us as a path-finder throughout this paper, and since no paper has so far reviewed this object at optical wavelengths, we will start with a quick overview of spectroscopic and photometric properties of SU Lyn. These are based on the very intensive monitoring we are keeping of the object since the preparatory phase leading to the Mk16 discovery paper, and whose results will be presented and discussed in detail elsewhere. The properties of SU Lyn that will be reviewed here are those that we will look for in the dataset of GALAH stars with the aim to discover the new SySt.

The two most obvious distinctive characteristics of optical spectra of SU Lyn (and *acc*-SySt of that type) are shown in Fig. 1: (a) a near-UV ultraviolet excess ($\lambda \leq 4000 \text{ \AA}$), and (b) weak emission lines, primarily from the hydrogen Balmer series. They both originate in the accretion disk forming around the degenerate companion, fed by the material accreted from the mass-losing RG companion.

Both can vary greatly in time, as the two epochs compared in Fig. 1 illustrate well: in just over one year SU Lyn passed from an *active* state (Dec 19, 2015), when its SySt nature was quite obvious, to a *quiet* phase (Feb 16, 2017) during which an optical spectrum would not have betrayed its binary nature. This needs to be kept in mind when comparing GALAH spectra with ancillary data taken at very different epochs.

The most important role of SU Lyn in guiding our search among GALAH stars is however the observed profile for emission lines, $H\alpha$ in particular. Fig. 2 presents a temporal sequence from Asiago 1.82m and Varese 0.84m telescopes + Echelle spectrographs illustrating the great variety of profiles observed for $H\alpha$ in this star from 2015 to 2020 (for a more traditional presentation of some of these same profiles for key epochs see fig. 3 of Munari 2019). The orbital plane of SU Lyn is probably close to face-on conditions and

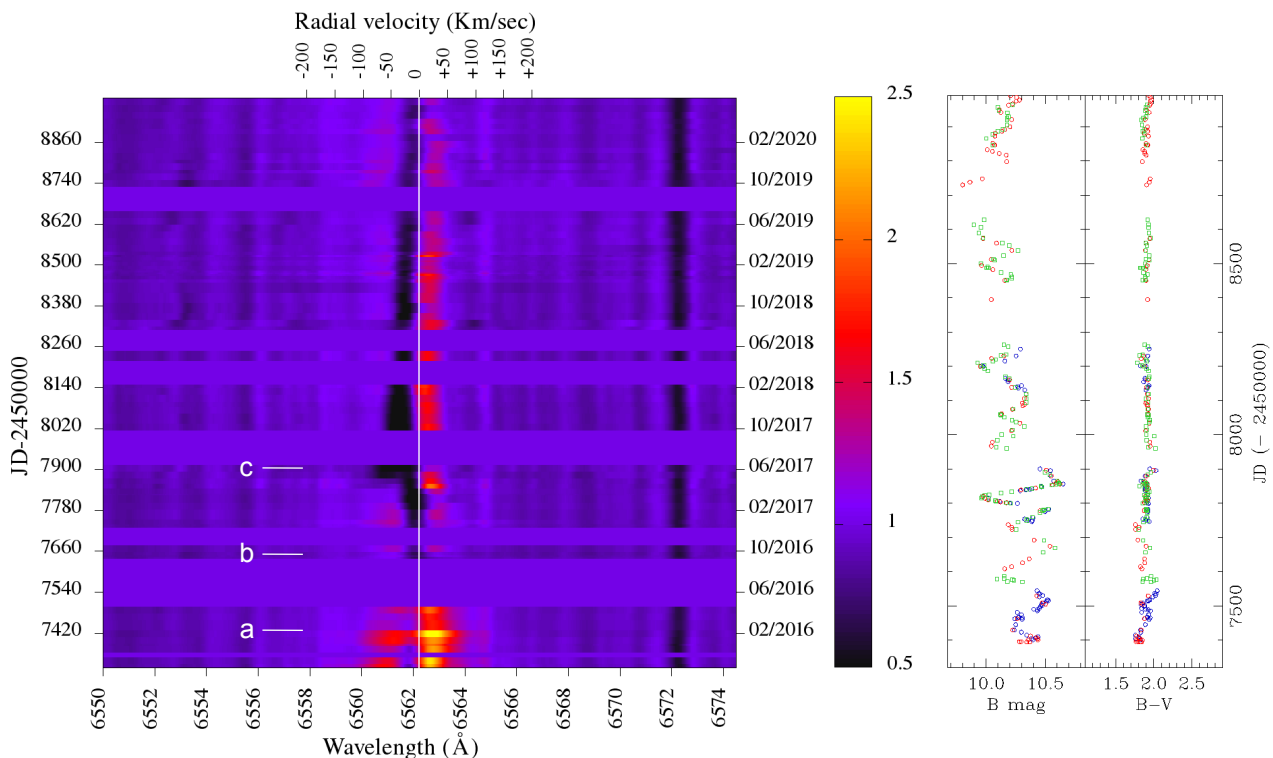


Figure 2. Temporal sequence from Asiago 1.82m and Varese 0.84m Echelle spectra (aligned in heliocentric wavelength) illustrating the great changes observed in the $H\alpha$ profile of prototype SU Lyn since its recognition in late 2015 as an accreting-only symbiotic star. The vertical line marks the $H\alpha$ rest wavelength at the stellar systemic velocity (-24 km s^{-1}). The epochs *a*, *b* and *c* are discussed in the text (Section 3). On the right the corresponding B,V lightcurve of SU Lyn as built from ANS Collaboration observations.

this accounts for the negligible changes in radial velocity observed for the M6III absorption lines ($\leq 2 \text{ km s}^{-1}$). The observed spectroscopic and photometric changes are therefore not related to changes in the aspect angle of the binary.

The epoch marked *b* in Fig. 2 corresponds to the lowest accretion rate and it is noteworthy for the absence of emission in $H\alpha$ and a null near-UV excess: at optical wavelengths SU Lyn appears like a normal and single M6III, not as an interacting binary. Only the reduced equivalent width of the $H\alpha$ absorption (only about half the photospheric value of typical M6III giants) and its narrow FWHM (again half the value for normal M6III giants) could cause doubt. The white vertical line in Fig. 2 represents the photospheric velocity of the cool giant: on epoch *b*, the velocity of the $H\alpha$ absorption almost equals that of the M6III giant. This is not the case for most of the time, however: as clearly shown by Fig. 2, the $H\alpha$ absorption is normally blue-shifted compared to photospheric absorptions as if originating in a gentle wind blowing off the inner regions of the accretion disk (and thus appearing superimposed onto its emission), or forming in the expanding wind of the RG that engulfs the whole binary system.

Epoch *c* in Fig. 2 marks the sudden appearance of a second, distinct and faster moving absorption component, that gradually reduced its velocity during the following months and finally merged with the slower, pre-existing absorption component. At the time of maximum equivalent width of this second absorption component, the emission in $H\alpha$ briefly vanished.

Finally, epoch *a* represents the condition of highest accretion rate, with a strong near-UV excess and a prominent and structured emission in $H\alpha$, with still superimposed the blue-shifted absorption component mentioned above. It is a lucky circumstance that when

we first observed SU Lyn in preparation of Mk16 paper, the star was exhibiting a clear emission in $H\alpha$ and the strongest near-UV up-turn: if at the time, it had appeared as in epoch *b* of Fig. 2, we could not have recognized it for what it really was.

Another important point illustrated by Fig. 2 concerns the photometric activity of SU Lyn. The star is too bright to be recorded unsaturated by surveys which monitor the heaven on a nightly basis in search for transients (eg. ASAS-SN, MASTER, ZTF, etc.), therefore we monitored it ourselves with small instruments, and fully transformed the observations to the Landolt (1992) standard UBVR system. As illustrated by the B,V lightcurve on the right panel of Fig. 2 (synchronized to the same temporal ordinates as the spectra to the left), SU Lyn varies by up to 0.7 mag amplitude in a random fashion, with no persistent periodicity. There is no associated change in colour and no correspondence with the behavior of the accretion disk as traced by $H\alpha$ intensity and profile. Thus, the variability is not caused by brightening and fading of the accretion disk (hotter than the M6III), but must originate with the cool giant. All cool giants exhibit variability to some extent (Hoffmeister, Richter, & Wenzel 1985; Sterken & Jaschek 2005), given the unstable nature of their convective outer layers (Pugh, Gray, & Griffin 2015), and their tenuous atmosphere that extends across the temperatures for molecule formation and through those for dust condensation. The absence of radial velocity variability on the left panel of Fig. 2 precludes an origin of the variability seen in SU Lyn with the coherent, large scale, persistent radial pulsations of the type observed in Mira long-period variables. The latter show a sinusoid-like radial velocity curve of $\sim 10\text{--}15 \text{ km s}^{-1}$ in amplitude, in phase with the equally sinusoid-like lightcurve that can span up to 10 magnitude in amplitude, and

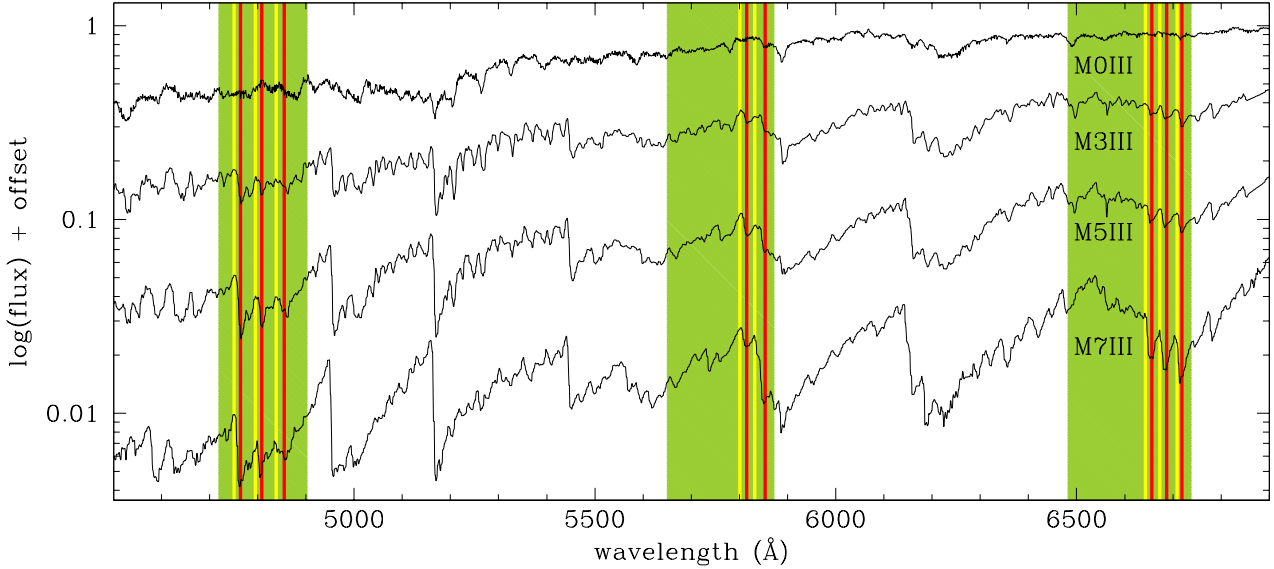


Figure 3. Definition of TiO classification indexes. The shadowed regions show the wavelength ranges covered by the GALAH blue, green and red channels. The yellow and red bands mark the A-B and C-D wavelength intervals, respectively, used to compute the b , g and r ratios according to Eq.(2) and Table 3. In background some Asiago 1.22m spectra illustrating the progress in strength of TiO bands moving along the sequence of M giants (pay attention to the log-scale of the ordinates).

characterized by bluer colour at maximum and redder at minimum (see fig. 27 in Hoffmeister, Richter, & Wenzel 1985).

The distinction with radially-pulsating giants is important: their outer layers experience large scale motions that lead to shocks, which in turn power emission lines. In our search for *acc*-SySt we aim to avoid the contamination from radially-pulsating giants and their deceiving emission lines. The selection criteria for removing false positives from the final *acc*-SySt sample are outlined in the rest of the paper.

4 SELECTION STEPS

Our search for *acc*-SySt among GALAH targets started with isolating the cool giants from the rest. In this paper we focus on giants of the M spectral types, those most abundant ($\sim 70\%$) among the known SySt (see the catalogs by Allen 1984, Belczyński et al. 2000, Akras et al. 2019, Merc, Gális, & Wolf 2019b). SySt containing other types of cool giants will be explored in follow-up papers.

4.1 Colour

The intrinsic colour of M0 giants in the Solar neighborhood is $(J - K)_o = 0.97$ (Lee 1970; Koornneef 1983), so we first apply a colour selection of $(J - K_s) \geq 0.90$ to GALAH targets to both account for the natural spread with the breadth of the M0 spectral type and the slight difference in wavelength-baseline between the Johnson’s $(J - K)$ and 2MASS $(J - K_s)$ indices.

4.2 Parallax

On the HR diagram, stars with an M spectral type are either very low-mass main sequence objects (down to the limit for stable H-burning in the core), or giants resulting from the evolution of more massive progenitors. The stars in our Milky Way have not lived

Table 2. Parallax for dwarf and giant M stars (under negligible reddening) at the bright ($V=12$) and faint ($V=14$) end of the GALAH magnitude range.

	M_V	parallax (mas)	
		V=12	V=14
M0V	8.90	24	10
M5V	12.30	115	46
M0III	-0.10	0.38	0.15
M5III	-0.90	0.26	0.10

long enough to significantly populate the range in between. M-dwarfs are intrinsically very faint and over the $12 < V_{JK} < 14$ mag range covered by GALAH targets, they represent the stars closest to the Sun, while the opposite is certainly true for the giants. In Table 2 we compare (under negligible reddening) the expected parallax of dwarfs and giants with an M spectral type at both ends of the GALAH magnitude range. No giant has a parallax larger than 0.4 mas, or a dwarf smaller than 10mas. Therefore a second criterion was set imposing a Gaia DR2 (Gaia Collaboration et al. 2018) parallax $\pi \leq 3$ mas. This selection criterium is fully confirmed by the improved Gaia eDR3 parallaxes (Gaia Collaboration 2020), that became available only after this paper was originally submitted.

4.3 TiO absorption bands

The above colour and parallax criteria combined together returned an initial sample of 29 514 GALAH stars. This sample could contain hotter giants of G and K spectral types affected by a large reddening or cool giants of a spectral type other than M (like the Carbon giants). To prune them out and retain only those with an M-type spectrum, we looked for signatures of their distinctive TiO absorption bands in the GALAH spectra. This may have picked-up also some S-type giants whose spectra, in addition to TiO bands, show also molecules involving s-type elements (ZrO in particular; Turnshek et al. 1985).

Table 3. Short and long wavelength limits (Å) of the intervals used to compute the ratios in Eq. (2) and illustrated in Fig. 3.

ratio	λ_A	λ_B	λ_C	λ_D
b1	4751	4756	4765	4770
b2	4798	4803	4807	4812
b3	4835	4840	4850	4855
g1	5801	5806	5812	5817
g2	5829	5834	5850	5855
r1	6641	6646	6653	6658
r2	6670	6675	6684	6689
r3	6706	6711	6716	6721

Some percentage of known SySt do indeed possess S-type giants (Jorissen 2003).

Fig. 3 presents a progression of M giant spectra with overplotted in green the wavelength range of the blue, green and red GALAH channels. Within their span lie strong TiO bands, and the later the spectral type, the deeper such bands become. To confirm the presence of the TiO bands and objectively derive their depth, we defined eight narrow TiO wavelength bins (marked in red in Fig. 3) and an equal number of control wavelength bins (marked in yellow in Fig. 3). The control bins are all placed to the blue of their respective TiO bins given the fact that absorption bands of the TiO molecule all degrade to the red and present a steep band-head to the blue (Pearse & Gaydon 1976). We then defined eight *ratios* (b1, b2, b3 in the blue channel, g1, g2 in the green, and r1, r2 and r3 in the red) by integrating the flux within the control bin and dividing by it the TiO bin as:

$$\text{ratio} = \frac{\int_{\lambda_A}^{\lambda_B} f(\lambda) d\lambda}{\int_{\lambda_C}^{\lambda_D} f(\lambda) d\lambda} \quad (2)$$

where the respective wavelength intervals A–B and C–D are listed in Table 3. These ratios were computed on spectra before continuum normalization but shifted to rest frame by the radial velocity listed in GALAH DR3 as `rv_guess` (Buder et al. 2020). Absence of absorption by TiO returns a value around 1.0 for any of the ratios, and a progressively larger value with increasing M spectral subtype (M0 → M10). Finally, we have combined the eight ratios into a single one computed as

$$f = \frac{[0.3(\langle b \rangle - 1) + 1] + \langle g \rangle + \langle r \rangle}{3} \quad (3)$$

where $\langle b \rangle$ stands for the arithmetic average of b1, b2 and b3, and similarly for the rest. The $\langle b \rangle$ average ratio stretches over $3.3\times$ the range of the other two, so we have consequently reduced its impact to make it equal to the others. This is justified by the lower S/N of the spectra recorded in the blue channel compared to green and red ones.

The depth of the TiO bands has been already used in the past to classify the M giants of symbiotic stars, e.g. by Kenyon & Fernandez-Castro (1987) that used to this aim the bands at 6180 and 7100 Å (both outside the GALAH wavelength range). In these studies, equivalent widths of TiO bands were measured over their entire wavelength span (hundreds of Å), too wide compared to the breadth of GALAH channels, and therefore inapplicable in the present paper (and for that matter also to more conventional, high-resolution Echelle spectra covering too small a wavelength interval over a single order).

Table 4. Intervals in combined f -ratio (Eq. 3) defining the template bins for the selected 15 824 M giants. $(J - K_s)_0$ is the median value within the bin for the reddening corrected $(J - K_s)$ from 2MASS, and $M(K_s)$ is the median value of the absolute magnitude computed from Gaia *e*DR3 parallaxes satisfy the condition $\sigma(\pi)/\pi < 0.1$. The last column lists the number of stars in each bin. The template spectra for each bin are plotted in Fig. A1.

bin	left limit	right limit	$(J - K_s)_0$	$M(K_s)$	N. stars
00	1.0200	1.0303	0.904	-3.78	3419
01	1.0304	1.0419	0.935	-4.01	2309
02	1.0420	1.0561	0.968	-4.27	1732
03	1.0562	1.0736	0.994	-4.58	1424
04	1.0737	1.0950	1.017	-4.81	1282
05	1.0951	1.1214	1.043	-4.99	1200
06	1.1215	1.1539	1.065	-5.18	1048
07	1.1540	1.1938	1.088	-5.42	919
08	1.1939	1.2428	1.110	-5.69	917
09	1.2429	1.3030	1.141	-5.94	849
10	1.3031	1.3770	1.166	-6.12	638
11	1.3771	1.4679	1.182	-6.29	77
12	1.4680	3.6559	1.139		10

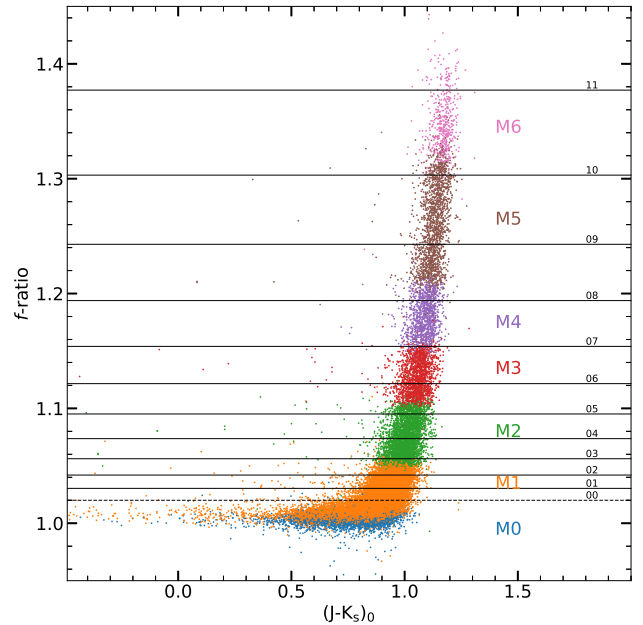


Figure 4. Relation between the reddening-corrected 2MASS $(J - K_s)_0$ colour index and the combined f -ratio from Eq.(2) for the 29 514 GALAH stars in our initial sample. The coloured bands mark the approximate location of the MKK spectral subtypes (M0III, M1III, ...). The finer, log-scale subdivision according to Table 4 is given by the horizontal lines and it is marked by the numbers to the right (00, 01, ...).

The way our ratios are defined, makes them insensitive to spectral fluxing, continuum normalization, or reddening. The relation between f -ratio and reddening corrected $(J - K_s)_0$ index for the initial sample of 29 514 GALAH stars is illustrated in Fig. 4. The latter shows a number of highly reddened stars contaminating the sample. To filter them out we took all stars laying above the knee at $f > 1.02$, and considered the remaining 15 824 objects (the 15k-sample for

short) as representing the true M-giants present among the 600 255 stars observed by GALAH at the time of writing of this paper. The $(J - K_s)_0$ colour index has been calculated from 2MASS photometry and the full extinction as given by [Schlafly & Finkbeiner \(2011\)](#). The choice of taking the full value of the tabulated extinction is justified by considering the great distance to our targets (typically several kpc, beyond which Gaia DR2 or *e*DR3 parallaxes become inaccurate) and their large galactic latitude, which makes their sight-lines exit the Galactic dust slab well before reaching them.

4.4 $H\alpha$ in emission

The next step has been searching the 15k-sample of true M giants for those showing $H\alpha$ (and $H\beta$) in emission. All the symbiotic stars considered in this paper show $H\alpha$ emission directly on the recorded spectrum, well before any reference spectrum is subtracted (cf. Fig. 5). To properly reconstruct the profile of the emission line, it is however necessary to subtract the underlying spectrum of the M giant. To define the latter, we grouped the M giants by similar strength of TiO bands, and computed the median of the continuum normalized spectra within each bin. The spectral progression of the templates around $H\alpha$ and $H\beta$ is compared in Fig. A1 of the Appendix.

We initially selected to define a unique template for each of the eleven M0 III \leftrightarrow M10 III spectral subtypes of the original MKK classification scheme ([Morgan, Keenan & Kellman 1943](#); [Morgan & Keenan 1973](#)), but quickly realized that at the high S/N and high resolution of GALAH spectra, any such sub-type spans too wide a range in stellar properties for a single template to adequately represent them all. Similarly, equally spaced bins in f -ratio are not satisfactory, as they oversample at low f values. Therefore, we decided for a logarithmic progression, with Table 4 listing the 13 final bins, their interval in terms of f -ratio, and the number of true M giants contained in that bin. Their subdivision of the giant branch is shown in Fig. 4 (horizontal lines). The median of all the spectra in a given bin defines the template spectrum for that bin. Taking the median value eliminates any disturbance from cosmic ray hits or rare presence of emission components. In addition, the median computed over thousands of individual spectra has an extremely high S/N and it is completely insensitive to chemical peculiarities of individual stars.

The template is finally subtracted from continuum normalized spectra of the true M giants within the given bin, and the residuals inspected for emission in $H\alpha$. In this first paper we limit ourselves to consider only the M giants showing an $H\alpha$ emission profile rising above a threshold of 0.5 on the subtracted spectrum. This returned a total of 223 stars.

4.5 Visual inspection

The spectra of these 223 stars were visually inspected for inconsistencies that could cause the $H\alpha$ to appear in emission on the subtracted spectrum.

Some spectra were found to suffer from a mismatch in radial velocity with the template. In these few cases, the radial velocity rv_guess from GALAH DR3, which is used to shift spectra in all four GALAH channels to rest frame, provides correct results for the blue, green, and infrared, but not for the red channel, resulting in an excess flux around $H\alpha$ in the difference spectrum, which is obviously spurious.

Another, more frequent cause for false positives was the presence of an emission component probably originating from the

sky background that has not been fully cancelled-out by the sky-subtraction procedure. This may happen e.g. when the target star is located in a region of the sky affected by diffuse background emission, like emission nebulae and HII regions. Such cases are easy to recognize because the $H\alpha$ and $H\beta$ emission lines are (a) typically quite sharp, single-component and symmetric, (b) frequently accompanied by [NII] 6548, 6584 nebular emission lines (which do not form in the high density environment of an accretion disk), and (c) usually displaced in velocity with respect to the M-giant spectrum by an amount larger than expected from orbital motion in a symbiotic binary. In multi-fibre spectroscopic surveys like GALAH, only a limited number of fibres are assigned to record the sky background. They are distributed over the field of view away from the position of known stars. This is perfectly fine for a great fraction of the sky away from the Galactic plane. There are however, here and there, regions of the sky affected by background emission due to diffuse nebulousity. The intensity of such emission may vary appreciably over limited angular distances, and the same may be the case for the internal nebular gas dynamics and therefore the resulting wavelength for $H\alpha$ and $H\beta$ emitted lines. Any sparse mapping realized by a limited number of sky fibres of such a complex 2D pattern can naturally result in non-null residuals of the sky-background subtraction, in addition to other caveats of sky subtraction as explained in [Kos et al. \(2017\)](#).

There was also a group of stars which presented an equal excess emission in $H\alpha$ and $H\beta$ on the subtracted spectrum, always with the same characteristic profile (steep red and blue ends, flat and rounded top), as if originating from a hydrogen deficiency compared with the template spectrum. These stars were also disregarded in the current selection process.

After a further few rejections for miscellaneous reasons, we were left with a final selection of 83 M giants showing genuine emission in $H\alpha$ with an intensity in excess of 0.5 in the subtracted spectrum (the 83-sample hereafter). Stars with an emission in $H\alpha$ weaker than 0.5, which are inherently more subtle to treat, will be investigated in a follow-up paper.

4.6 Filtering out the radial pulsators

Not all the objects in the 83-sample are necessarily valid *acc*-SySt. The main false-positives are expected to be the (large-amplitude) radial pulsators (e.g. Miras or SRa variables), that may give origin to emission lines (primarily hydrogen Balmer) deep in their atmosphere where shocks form.

It is of course not precluded that a Mira pairs with a compact companion to form a symbiotic star. For example V407 Cyg, prior to its 2010 nova outburst, was primarily studied as a Mira suffering from possible dust-obscuration episodes ([Munari, Margoni, & Stagni 1990](#); [Kolotilov et al. 1998](#)) with little (or none) spectroscopic evidences for binarity ([Hinkle et al. 2013](#)). *Mira* itself (= *o* Cet) is a well known *acc*-SySt: HUBBLE in the ultraviolet and CHANDRA at X-rays have spatially resolved its WD companion, the accretion disk and the stream fueling it ([Karovska 2006](#)). Such a plethora of multi-wavelength information is however not available for a typical GALAH anonymous star, and to be on the safe side we decided - at the initial stage of our project represented by this paper - to filter out the radial pulsators. Such a pruning is based on converging photometric (lightcurve) and spectroscopic ($H\beta/H\alpha$ emission ratio) criteria, described below.

We decided not to rely on existing compilations of known vari-

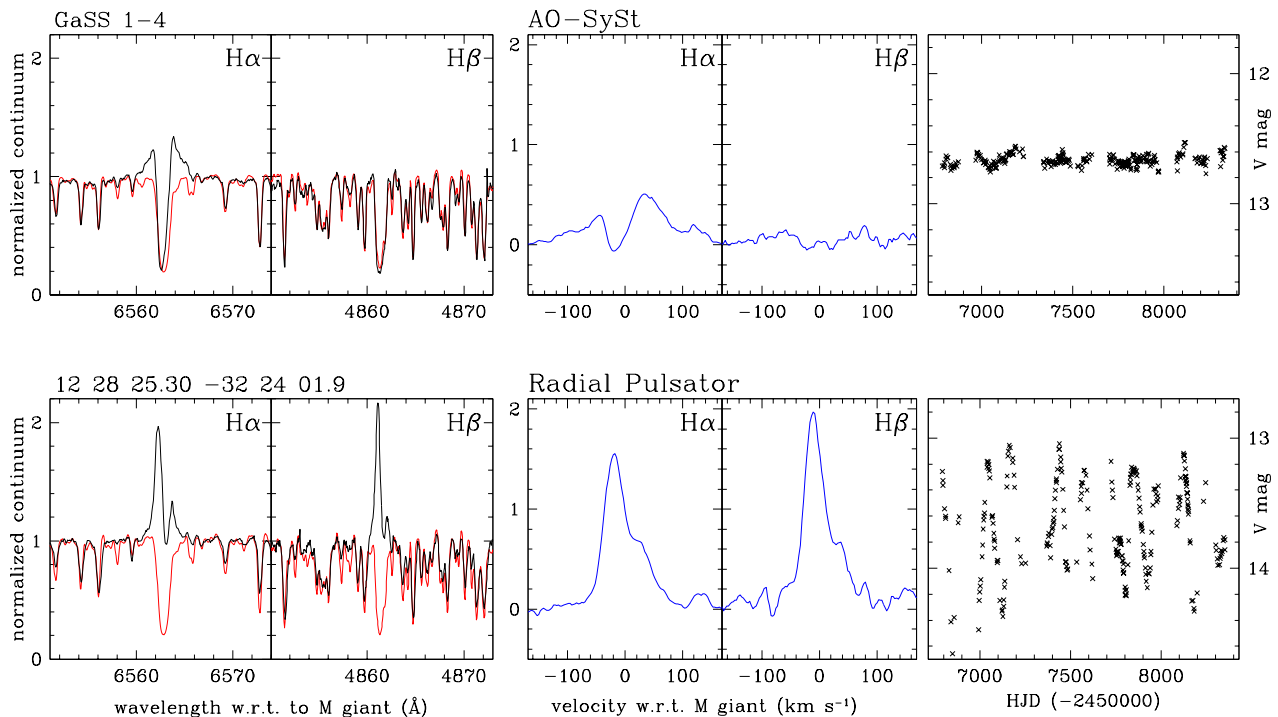


Figure 5. *Left-most panels:* example $H\alpha$ and $H\beta$ profiles (in black) from RV-zeroed GALAH spectra of a symbiotic star (top row) and of a radial pulsator (bottom row), compared with those of the template for the same f -ratio bin (in red, cf. Table 4). *Center panels:* the result of subtracting the (red) template spectrum from the (black) object spectrum from the left panels. *Right-most panel:* the corresponding V -filter lightcurve from ASAS-SN sky patrol data.

ables (as for example collected in the VSX¹ catalog), because the adopted classification criteria (as well as amplitude and periods) are sometimes in disagreement among themselves and also in conflict with the naming conventions listed in the IAU General Catalog of Variable Stars². We preferred instead to analyze in a homogeneous way their photometric behavior ourselves. To this aim we downloaded the available photometry for the 83-sample from the ASAS-SN sky patrol survey (Shappee et al. 2014; Kochanek et al. 2017) and examine ourselves the resulting lightcurves, which are usually composed of hundreds of individual observations in either g or V bands distributed over a time-interval of a few years, and therefore adequate to reveal the presence of long and stable periodicities related to radial pulsation. ASAS-SN sky patrol covers the whole accessible sky on both hemispheres every night, and the $12 < V_{JK} < 14$ mag range of our targets is ideally placed at the center of ASAS-SN dynamic range, away from the bright saturation limit or the noisy detection threshold.

The lightcurve of a Mira shows regular, long period (from several months to longer than a year) and large amplitude (from a few to >10 magnitudes) sinusoid-like variations (e.g. Hoffmeister, Richter, & Wenzel 1985; Sterken & Jaschek 2005). The large scale radial pulsation is betrayed by the in-phase variation of the radial velocity of the absorption spectrum, with amplitudes of the order of ~ 10 - 15 km/s (Joy 1926; Hoffmeister, Richter, & Wenzel 1985). Our path-finder SU Lyn shows a significant variability (0.6 mag amplitude in V), but it lacks the larger amplitude and the regular beat of a Mira. As clearly illustrated by Fig. 2, the M giant in SU Lyn does not radially pulsate in any significant way (the absorption lines are stable in radial velocity

to better than 2 km s^{-1}), and therefore no shocks form in the atmosphere which could lead to emission in the Balmer lines. Armed with these considerations, and to stay on the cautionary side, we selected to flag (in the 83-sample) all the stars showing ASAS-SN lightcurves with an amplitude in excess of 0.7 mag and a stable and clean sinusoid-like shape (cf. Fig. 5). Such a lightcurve could however arise also from orbital motion, for example from ellipsoidal distortion when the cool giant fills its Roche lobe and/or its side facing the companion is irradiated and heated up (e.g. as in the accreting-only and recurrent nova T CrB; Munari, Dallaporta, & Cherini 2016). A spectroscopic confirmation of the radially pulsating nature is therefore required, and this needs to be accommodated within the single-epoch spectra (i.e. no revisit) of the GALAH survey.

In radially-pulsating cool giants, outward moving material collides against the gas lifted during the previous cycle and now falling back inward. The resulting shock is hot enough to excite emission in the Balmer lines of hydrogen. Such shocks develop deep within the atmosphere, interior to the outer layers where absorption by TiO molecules occurs. The absorption by TiO begins around 4200 \AA and, by superposition of successive bands (they all decline toward the red), their combined absorption grows rapidly stronger with wavelength (Fluks et al. 1994). As a consequence, emission in $H\delta$ (4101 \AA) and higher Balmer terms exits the atmosphere unscathed by TiO, and their flux declines with increasing upper n -quantum number in the usual way. What happens to the red of $H\delta$? Going from $H\gamma$ to $H\beta$ and then $H\alpha$, we move into deeper and deeper overlapping absorption by TiO bands and the *observed* emission in the line becomes more and more absorbed. Saying it a different way (Joy 1926; Yamashita & Nariai 1977), in pulsating M giants the strongest line is $H\delta$ and the intensity of successive Balmer emission lines declines *either* going to the blue or to the red (see exemplary spectrum for LQ Sgr presented by Bragaglia et al. 1995). In most astrophysical

¹ <http://vizier.u-strasbg.fr/viz-bin/VizieR-3?-source=B/vsx/>

² <http://www.sai.msu.su/gcvx/>

environments, the observed emission in $H\alpha$ is invariably stronger than in $H\beta$, while in Miras the opposite is the case (Merrill 1940), because of the TiO absorption in the outer atmospheric layers. This offers a clear distinction between the emission originating from the accretion disk in an *acc*-SySt (in terms of equivalent widths: $EW(H\alpha) > EW(H\beta)$) from that expected to come from the internal shock regions of an M-type radial pulsator ($EW(H\alpha) \leq EW(H\beta)$).

GALAH high-resolution spectra show a further distinction between the two types. In *acc*-SySt systems, a sharp absorption component appears superimposed to the broad $H\alpha$ emission profile, generally *blue-shifted* by about 5–25 km s⁻¹ and half as wide as the photospheric $H\alpha$ absorption line (FWHM~15–25 km s⁻¹ as opposed to 45–50 km s⁻¹), that - by analogy with the prototype SU Lyn or other *acc*-SySt discussed by Jorissen et al. (2012) and Gorlova, Van Winckel, & Jorissen (2012) - is believed to originate in the gentle wind blowing off the accretion disk or in the outflowing wind of the RG that engulfs the whole binary system. In the GALAH spectra of radially pulsating stars, the narrow absorption superimposed to the emission is instead generally *red-shifted* as if coming from cooler material falling back toward the star after being lifted higher up during the previous pulsation cycle.

These photometric and spectroscopic criteria to separate *acc*-SySt and radially pulsating objects in the 83-sample are illustrated in Fig. 5, which presents line profiles and lightcurves well typical of the rest of the sample: high-amplitude and regular beating for the lightcurve of a pulsator, with strong $H\beta$ and red-shifted narrow-absorption; lower amplitude and less regular lightcurve for the *acc*-SySt, an $H\beta$ much weaker than $H\alpha$ and blue-shifted narrow-absorption. By applying these criteria, 30 radial pulsators are pruned from the 83-sample, reducing the candidates *acc*-SySt to 53. Hereafter, we refer to them as the 53-sample.

4.7 Avoiding contamination by T Tau stars

T Tau pre-main sequence variables have been considered as possible contaminants in previous large-scale searches for new SySt, especially those based on IPHAS $r,i,H\alpha$ photometric survey (Corradi et al. 2008, 2010, 2011; Rodríguez-Flores et al. 2014). T Tau stars are distributed over a wide range of spectral types, from mid-F down to the coolest M-types, may be heavily reddened, and present emission lines originating from the circumstellar disk, the spotted surface and the magnetic-confined accretion columns on the magnetic poles (Hartmann, Herczeg, & Calvet 2016). T Tau stars can therefore mimic the red $r-i$ colour of SySt and similarly stand out in the $r-H\alpha$ photometric index. T Tau stars are less prone to be confused with SySt if spectra are available, especially if they cover a broad wavelength range (as those we have collected in Section 5.1 below for our program stars): the spectra of T Tau stars show the absorption features typical of a main sequence star, not of a giant, and the emission lines are rather different both in assortment (CaII H & K doublet usually quite strong in T Tau stars, while generally absent in SySt) and in their profile (in T Tau stars sporting narrow jet components superimposed on a broad pedestal coming from the rotating disk; Giannini et al. 2019). In addition, LiI 6707 Å is in strong absorption in most T Tau stars, whereas it is generally absent in SySt.

In the context of our search for new SySt, T Tau stars are however of no concern, because they cannot be confused with cool giants when the segregation is carried out on Gaia parallaxes, as we did. Of relevance to the present paper are only T Tau stars with an M spectral type (M-TTtau for short). The intrinsically brightest among M-TTtau are those with the earliest M-types, M0V and M1V. The

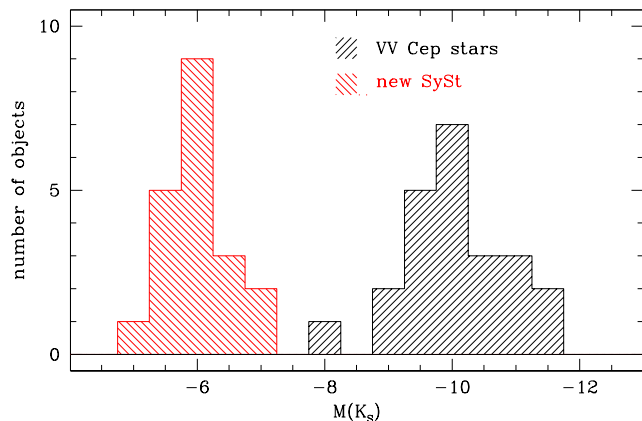


Figure 6. Distribution in $M(K_S)$ for the program new SySt compared to that of VVCep stars.

absolute magnitude of M0V and M1V stars are $M(V)=8.8$ and 10.8 , respectively, while that of M0III and M1III giants is $M(V)=-0.5$ (Drilling & Landolt 2000; Sowell et al. 2007). The inflated photospheric radius (not yet settled on the main sequence) and the contribution by the circumstellar disk may raise the intrinsic brightness of M-TTtau above that of single and isolated dwarfs of the same spectral type, but they will never fill the huge ≥ 10 mag gap between main-sequence and giant stars of the M spectral type.

In confirmation of this, we have retrieved the Gaia *e*DR3 parallaxes for the brightest known M-TTtau (selected from the compilation by Yang et al. 2012) and computed their $M(V)$ magnitudes by adopting the photometric calibration of the Gaia Consortium (Evans et al. 2018). The absolute $M(V)$ magnitudes of M-TTtau turned out to be all fainter than +6.5, confirming that in no way an M-TTtau may have slipped into our sample of M giants segregated on the base of Gaia parallaxes (see also Section 5.9 below). As a further check, we took the compilation of T Tau stars listed in SIMBAD and VSX, and checked if any matched the M-giants of the initial 15k-sample, and verified that none did.

4.8 Comparison with VVCep binaries

There are binaries which host cool supergiants and massive hot companions, of which a comprehensive catalog of 108 Galactic objects has been recently published by Pantaleoni González et al. (2020). The 23 entries from this catalog with an M spectral type for the cool giant are summarized in Table A5, where we add distances, absolute magnitudes and height above the galactic plane as derived from Gaia *e*DR3 parallaxes and the 2MASS JHK_S survey. Such objects are usually named VVCep stars, from the best known member of the group, and while not related to SySt are sometimes discussed in parallel. We have not included δ Sge in Table A5 as it seems more related to other types of objects like TX CVn or 17 Lep than to VVCep stars (Ginestet & Carquillat 2002; Pugh, Gray, & Griffin 2015).

The VVCep stars all have very massive components on very wide orbits. The orbital solution for VV Cep itself gives an orbital period of 20.3 yrs, an orbital separation of 24.8 AU, and individual masses of $18.2 M_{\odot}$ and $18.6 M_{\odot}$ for the M supergiant and the B-type companion, respectively (Bennett et al. 2004). Of interest to us is the fact that in VVCep stars, the Balmer lines, and $H\alpha$ in particular, may be seen in emission, with a line profile reminiscent of that seen in Be stars (in which the emission comes from an equatorial ring-

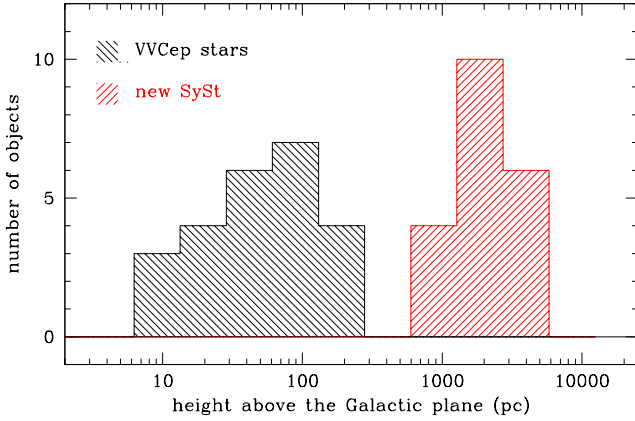


Figure 7. Distribution in height over the plane of the Galaxy for the program new SySt and for VVCep stars.

like shell formed by material leaving the hot star which is rotating close to break-up velocity). While the hot component in VVCep dominates the spectrum in the blue, that of the M supergiant takes over at red wavelength. With an $H\alpha$ in emission superimposed, it could be questioned whether any of our new SySt may indeed belong to VVCep stars. This, however, can be safely excluded on two independent grounds.

First, M supergiants of VVCep stars are intrinsically much brighter than the M giants characterizing our new SySt. The two are compared in Fig. 6, with values taken from Table A2 for the new SySt, and Table A5 for the VVCep stars. The median absolute $M(K_S)$ magnitude for VVCep stars is -10.0 , that of the new SySt only -5.9 . Secondly, their distance over the Galactic plane is radically different. Being very massive and therefore very young, VVCep are examples of extreme Pop I stars, laying close to the Galactic plane, while our new SySt belong to a much older population as discussed in Section 5.9 below. Their distributions in terms of height above the Galactic plane are compared in Fig. 7, with input data taken from Table A2 and Table A5: the median value is just 50pc for the VVCep stars and a much larger 1.8kpc for the new SySt.

5 THE FINALLY SELECTED 33 NEW SYMBIOTIC STARS AND THEIR PROPERTIES

We have finally subjected the 53-sample to a series of follow-up observations from the ground and the space to pick-up the most promising objects. Based on the ensuing results, our final list of 33 proposed *acc*-SySt candidates is presented in Table 5 (where GaSS in their names stands for Galah Symbiotic Star); they are divided in two groups, a primary and a supplementary sample. The division is based primarily on available follow-up observations (less for the supplementary sample) and amplitude of photometric variability (larger for the supplementary sample). A plot similar to Fig. 5, presenting the $H\alpha$, $H\beta$ profiles and the lightcurve, is provided in the appendix for all 33 objects (Fig. A2 to A8).

Gaia *eDR3* lists parallaxes (π) for all the 33 new SySt, and they are reported with their uncertainties ($\sigma(\pi)$) in Table A2. In Table 5 we provide distances, by direct inversion of parallax, for only 20 of them, namely those satisfying the condition $\sigma(\pi)/\pi < 0.2$. This is the limit recommended by the Gaia team (Bailer-Jones 2015; Luri et al. 2018). The parallaxes of the remaining program stars are too small in comparison to their formal uncertainties and even

generally smaller than the *mean* 0.019mas bias affecting Gaia *eDR3* parallaxes as a whole (Lindegren et al. 2020). Such bias depends in a non-trivial way on (at least) the magnitude, colour, and ecliptic latitude of the sources, with no firm correcting recipe available yet. Improved parallaxes in future Gaia data releases will allow to derive valuable distances to (most of) the remaining program stars.

We now describe the follow-up observations that have led us to the compilation of Table 5. A complete description of such extensive follow-up observations is far beyond the scope and breadth of the present paper. Full details, augmented by the results of further follow-up observations currently in progress, will be discussed elsewhere.

5.1 Near UV up-turn

The presence of a bright accretion disk is betrayed by an emission excess at wavelengths shorter than $\sim 4000 \text{ \AA}$, as illustrated for SU Lyn in Fig. 1. With the long-slit B&C spectrograph attached to the Asiago 1.22m telescope, highly efficient down to the atmospheric cut-off ($\sim 3200 \text{ \AA}$ at the 1000m above sea level location) we have observed most of the objects in the 53-sample located north of -29° in declination (Table A1 in the Appendix provides a log-book of these observations). At the Asiago $+46^\circ$ latitude, this corresponds to a horizon distance of 15 degrees. The near-UV faintness of the program stars and the high atmospheric extinction at such large air-masses conspired to make such observations quite demanding to execute. A consistent number of spectro-photometric standards were observed in parallel each night at similarly large air-masses. Suitably high S/N at $3400\text{-}3600 \text{ \AA}$ was obtained for only a fraction of the attempted objects, and sometimes only after adding spectra collected at different revisits. The objects marked "spc" in the U_{exc} column of Table 5 are those showing excess emission on spectra over the range $3400 \leq \lambda \leq 4000 \text{ \AA}$. There are clear hints for some of them that the amount of near-UV excess changes when spectra taken at different epochs are compared.

A quick summary of the photometric data extracted from spectra is presented in Fig. 8. The B and V data lie well on a 1:1 relation with APASS mean data, the scatter being at least in part related to the variability all objects display (as per column ΔV of Table 5). The difference in the $B-V$ colour (indicative of the accuracy of the *slope* of fluxed spectra) between APASS and spectra appears well distributed around 0.0 with a FWHM of about 0.1 mag. The most interesting panel of Fig. 8 is the last one, showing the distribution of $U-B$ measured on spectra compared with the distribution of $U-B$ for a hundred M giants of the Solar neighborhood (suffering from negligible reddening) as measured by Fluks et al. (1994). It is clear how, on average, the $U-B$ colour of candidate *acc*-SySt is bluer than those of (supposedly) single, normal M giants, supporting the notion that for a sizeable fraction of them we have actually observed an excess in U as coming from the companion and the accretion disk. The *acc*-SySt scoring an "spc" in Table 5 are those with an $U-B$ bluer than $+0.4$ in Fig. 8, and "spc:" for those between $+0.4$ and $+0.8$.

5.2 Radial velocity variability

Armed with evidence from Fig. 2 that the low amplitude, irregular variability affecting the M giant in SU Lyn does not reverberate into changes in radial velocity, we observed some of the 53-sample north of -25° in declination with the Echelle spectrograph mounted on the Asiago 1.82m telescope. The results are summarized in Table 6.

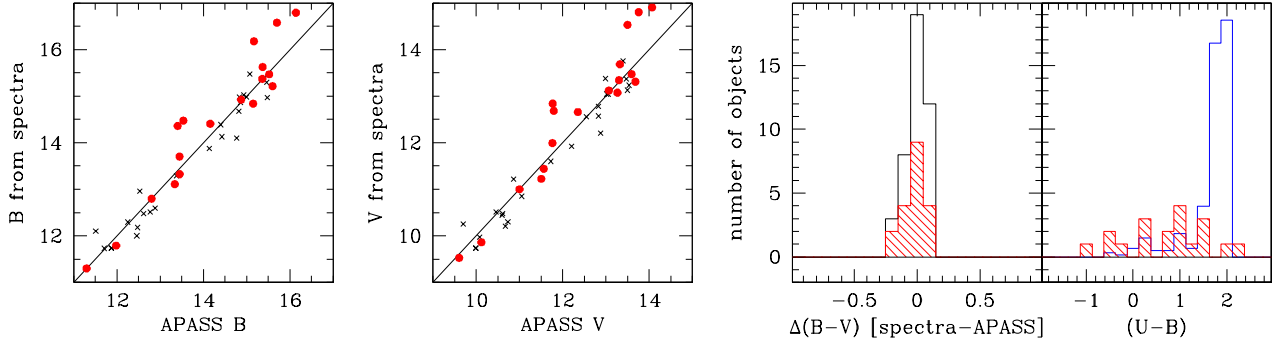


Figure 8. *Left-most panels:* comparison between the average B and V magnitudes from APASS all-sky survey, and the corresponding values derived from Asiago 1.22m flux-calibrated spectra for a subset of the 53-sample. The solid lines mark the 1:1 relation. *Right-most panels:* histogram distribution of differences between Asiago and APASS derived $B-V$ colours, and distribution of $U-B$ colours derived from Asiago spectra. The line in blue shows the distribution of a hundred M giants from the Solar neighborhood as measured by Fluks et al. (1994). Red colour refers to symbiotic stars discovered in this paper, black to other GALAH M giants observed along with them (including also some radial pulsators).

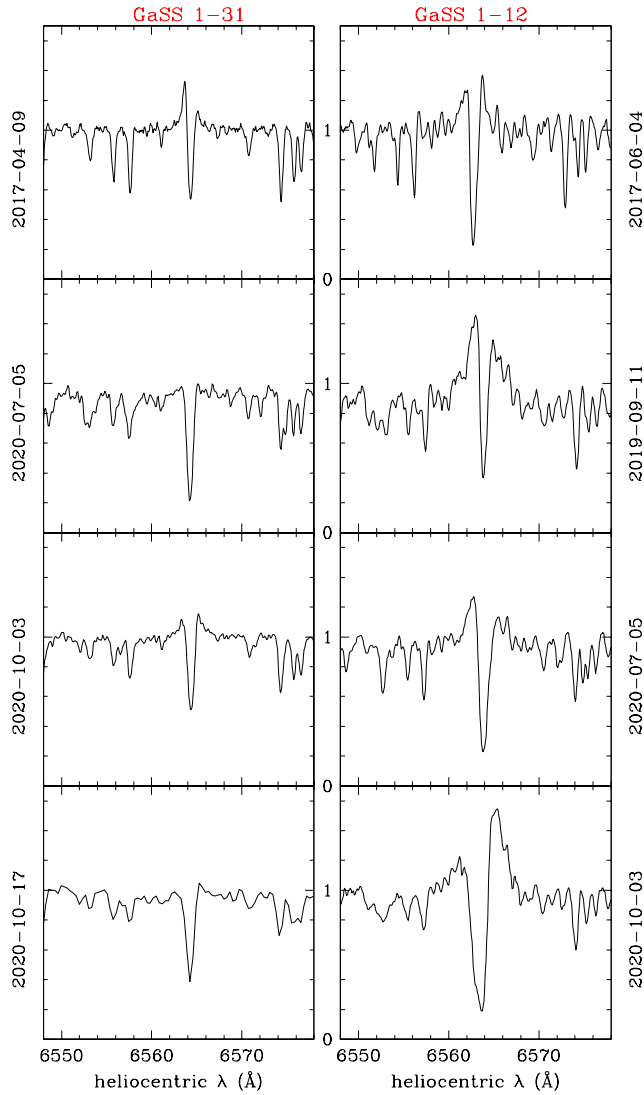


Figure 9. Example of variability observed on $H\alpha$ comparing the original GALAH spectra (top row) with Asiago 1.82m Echelle spectra obtained at later epochs (the left-bottom spectrum is from Varese 84cm telescope). Only GALAH spectra are corrected for telluric absorption lines.

As a check, some normal stars from the initial 15k-sample and a few radial pulsators from the 223-sample were also observed, with results presented in Table A3. In both tables, the quoted error for Asiago RVs is the *internal* error, i.e. that derived by comparing the RV obtained from different Echelle orders by cross-correlation with spectra of IAU radial velocity standards of M spectral type. We selected to limit the measurement to 5 of the 32 orders covered by the Asiago Echelle spectrograph, favoring those at redder wavelengths (where S/N is higher), and avoiding the orders with TiO bandheads or telluric atmospheric absorptions that would affect the cross-correlation results. A comparison of Asiago RVs with the GALAH rv_guess and Gaia DR2 values in Table A3 for the GALAH M giants sub-sample returns a negligible offset and an rms $\sim 1.5 \text{ km s}^{-1}$. The latter could in part be accounted by variability of epoch radial velocities intrinsic to the sources.

From the data in Table 6, a clear RV variability has been observed for five objects, and borderline for an additional three. They are marked with "var" in column "Asiago RV" of Table 5. We favor an interpretation in terms of orbital motion for this RV variability.

5.3 Emission line variability

The *acc-SySt* of this paper show a clear variability of the intensity and profile of $H\alpha$ emission line on spectra collected with the Asiago 1.22m and 1.82m telescopes. An example is presented in Fig. 9. GaSS 1-31 showed a clear emission in $H\alpha$ on the GALAH spectrum recorded on Apr 9, 2017, a weaker one on the Asiago spectrum for Oct 2, 2020, and no emission on Jul 5, 2020 (see also Section 5.5 below) and on Oct 17, 2020 (this last spectrum has been obtained at a lower resolving power - 12,000 because of 2×2 CCD binning - with an Echelle spectrograph mounted on the Varese 84cm telescope). The $H\alpha$ of GaSS 1-12 has been always observed in emission on all three visits with the Asiago 1.82m, with a varying degree of intensity and velocity of the emission relative to the M giant. Most interestingly, the last Asiago spectrum for Oct 3, 2020 shows the appearance of a second narrow absorption, blue shifted with respect to the primary one, an event reminiscent of what happened to SU Lyn in 2017 (cf. Fig. 2).

Table 5. The candidate accreting-only symbiotic stars (*acc*-SySt) discovered in this paper based on spectra from the GALAH survey. E(B-V) is from Schlafly & Finkbeiner (2011). The spectral type is on the MKK scale and f is the template label/bin (see Table 4 and Fig. A1). V is from the APASS catalog. ΔV is our estimate of the amplitude of variability on ASAS-SN sky patrol data (Section 4.6). 'P orb' lists possible orbital periods (for 2xP alternative see Section 5.7). 'dist' is the distance (in kpc) derived from Gaia e DR3 parallax for objects satisfying the conditions $\sigma(\pi)/\pi < 0.2$ (cf. Section 5). RV_{\odot} is from GALAH DR3 (rv_guess). Objects marked 'var' in the 'Asiago RV' column show a variability in radial velocity (cf. Table 6 and Section 5.2). The column 'Swift' marks with 'X' the objects counterpart to X-ray sources in the 2SXPS catalog (Evans et al. 2019), and with 'UV' those found emitting in the ultraviolet UVM2 band in our *Swift* follow-up observations (cf. Table 8 and Section 5.5). U_{exc} lists the presence of emission excess at U -band wavelengths: 'pht' from photometric UB observations (Massey 2002), 'spc' from our spectra (Section 5.1). An 'F' in the 'Flk' column marks the presence of flickering (Section 5.4). The final two columns provide the velocity (w.r.t. M giant) and the FWHM of the narrow absorption superimposed to the broader $H\alpha$ emission (Section 4.6).

name	RA (J2000)	DEC	Galactic		E(B-V) (mag)	spectral		V (mag)	ΔV (mag)	P orb (days)	dist (kpc)	RV_{\odot} (km/s)	Asiago RV	Swift	U_{exc}	Flk	$H\alpha$ (wind)			
			long	lat		type	f										RV	width		
<i>main sample</i>																				
GaSS 1-1	04 52 35.65	-70 40 42.7	282.35	-35.19	0.23	M1	03	12.950	0.23			+264.28				pht	F	-21.9	19	
GaSS 1-2	05 04 09.82	-70 12 17.6	281.44	-34.40	0.33	M2	04	12.725	0.43			+234.29				pht		-23.9	19	
GaSS 1-3	06 22 21.17	-59 39 26.9	268.79	-26.77	0.04	M0	00	12.521	<0.05		8.2	+282.99	X					-2.1	24	
GaSS 1-4	11 12 15.48	-32 07 19.3	279.61	26.22	0.10	M1	00	12.638	0.11	235	8.2	+141.44						-11.3	19	
GaSS 1-5	11 22 10.22	-29 21 12.5	280.56	29.61	0.05	M2	02	13.469	0.33	311	10.1	+35.75						-7.4	21	
GaSS 1-6	14 46 07.03	-37 53 38.7	326.64	19.64	0.06	M3	05	12.096	0.30	401	5.4	+33.35						-12.3	17	
GaSS 1-7	14 57 25.03	-24 48 24.8	336.07	29.84	0.13	M1	02	13.497	0.35			-235.14				spc		-9.3	24	
GaSS 1-8	15 23 54.79	-29 43 14.9	338.39	22.46	0.45	M1	00	13.637	0.16		7.4	-143.10						-17.1	24	
GaSS 1-9	16 55 28.75	-03 09 45.0	15.77	23.92	0.27	M1	02	13.299	0.28			-131.58	var:			spc	F	-7.2	11	
GaSS 1-10	17 07 24.58	-58 29 21.7	331.48	-10.65	0.15	M1	02	12.568	0.21			-100.12						-4.5	22	
GaSS 1-11	17 50 33.15	-47 22 40.4	344.53	-10.21	0.14	M3	06	12.182	0.09	453	6.6	+58.19		UV		F:		-22.0	27	
GaSS 1-12	18 57 06.98	-22 16 56.1	13.46	-11.15	0.22	M4	07	11.761	0.85		4.6	+51.88	var	UV		spc:		-11.4	14	
GaSS 1-13	19 27 26.71	-07 21 02.4	30.41	-11.33	0.32	M1	01	13.681	0.20	328		-373.27	var			spc	F	-13.5	19	
GaSS 1-14	20 37 56.95	+00 27 53.7	46.25	-23.28	0.06	M2	05	13.019	0.52	381	8.6	-247.79	var:			spc:		-6.4	21	
GaSS 1-15	21 10 01.51	+04 02 35.4	54.32	-28.20	0.08	M2	04	12.054	0.09	229	2.9	+49.94	var	X				-8.1	22	
<i>supplementary sample</i>																				
GaSS 1-16	05 31 40.32	-66 42 40.2	276.75	-32.60	0.10	M1	02	13.415	0.09			+302.18						F	-17.7	25
GaSS 1-17	07 06 36.52	-58 41 12.7	269.18	-21.04	0.09	M1	00	11.439	0.24		5.4	+119.77							-2.4	24
GaSS 1-18	12 08 19.12	-38 16 37.7	293.70	23.82	0.06	M1	02	13.068	0.33	338	8.7	+164.65							-16.9	26
GaSS 1-19	14 37 11.36	-78 36 33.9	308.20	-16.84	0.11	M1	01	13.422	0.15			+247.20							-7.1	26
GaSS 1-20	16 00 54.84	-16 28 32.5	355.07	26.66	0.25	M1	00	12.116	0.59			+44.76	var						-10.2	17
GaSS 1-21	16 12 42.83	-20 37 23.6	353.80	21.79	0.29	M4	06	13.757	0.70			-182.82				spc	F	-0.3	18	
GaSS 1-22	16 14 17.67	-25 09 20.4	350.53	18.44	0.27	M1	00	11.907	0.32		5.8	-242.25							-8.2	31
GaSS 1-23	17 11 24.39	-12 14 19.9	9.87	15.73	0.44	M4	07	13.321	0.68		4.8	-167.23	var:			spc		-4.6	22	
GaSS 1-24	17 17 44.36	-61 38 05.3	329.57	-13.48	0.09	M6	11	13.000	0.75			+171.01							2.5	19
GaSS 1-25	17 18 59.65	-17 47 37.5	6.13	11.14	0.23	M0	00	11.561	0.17		4.3	-81.87						F	-5.4	29
GaSS 1-26	18 07 34.98	-42 47 42.3	350.08	-10.60	0.10	M3	05	13.508	0.32			-1.74						F	-10.3	25
GaSS 1-27	18 32 00.28	-46 00 36.9	348.98	-16.00	0.06	M1	00	11.113	0.29	400	4.7	-42.51							-5.5	14
GaSS 1-28	19 01 02.81	-27 19 19.0	9.13	-14.03	0.20	M2	04	13.265	0.63	496	7.5	-106.75				spc		-4.8	21	
GaSS 1-29	19 08 07.66	-47 44 06.7	349.44	-22.40	0.07	M2	04	14.585	0.33		7.0	+149.28							-4.3	23
GaSS 1-30	19 11 35.88	-35 10 50.8	2.41	-19.06	0.07	M0	00	11.120	0.21		5.6	-48.38							-6.1	20
GaSS 1-31	19 17 16.24	-22 02 53.2	15.65	-15.30	0.10	M1	02	11.505	0.54		4.3	+70.13	var						-2.6	14
GaSS 1-32	19 18 43.66	-29 15 29.8	8.82	-18.37	0.11	M1	01	11.444	0.21		5.3	-95.48							-10.1	23
GaSS 1-33	22 10 02.95	-06 18 07.2	53.99	-46.41	0.05	M1	02	15.434	0.41	682		-205.14				spc	F	-11.7	15	

5.4 Optical flickering

The accretion in binaries is characterized by chaotic processes (e.g. density fluctuations in the accretion flow from the donor to the accreting star) that develop on time scales (seconds, minutes or a few hours) much shorter than those of other sources of variability (orbital motion, pulsation, rotation, outbursts, etc.). The possibility to detect flickering on optical photometric data depends primarily on its contrast with the steady sources in the system: the fainter the two components of the binary, the easier for flickering to become observable (e.g. Hellier 2001). Therefore, if flickering is easy to observe in cataclysmic variable stars that radiate about $1 L_{\odot}$ at optical wavelengths, it is an entirely different matter for symbiotic binaries in which the optical luminosity of the cool giant alone amounts to $10^2 L_{\odot}$.

The regions in the disk responsible for flickering are hot (Warner 1995; Zamanov et al. 2020), and their emission is con-

sequently rising toward the blue; that of the giant rises instead toward the red. Therefore, to reduce the background glare of the giant it is convenient to go as blue as possible (Skopal 2005). Detection of flickering at satellite ultraviolet wavelengths is straightforward as demonstrated by the *Swift* observations of SU Lyn by Mk16. On ground-based observations, the bluest photometric band is U (in its many variants: Landolt's U , u from Stromgren, or SLOAN u'). U band was relatively easy to observe in the old times of photo-electric photometers mounted on all-reflecting telescopes with bare-aluminum surfaces, thanks to the high instrumental throughput (no coatings or refractive components) and the excellent sensitivity of photo-multipliers like the standard RCA 31034A and Hamamatsu R934-02. Many searches for flickering in symbiotic stars were performed at that time (e.g. Slovak & Africano 1978; Mikołajewski et al. 1990; Tomov et al. 1996). The advent of CCDs, with their much lower sensitivity

Table 6. Heliocentric radial velocity of candidate GALAH symbiotic stars measured with the Asiago 1.82m telescope + Echelle spectrograph compared with the corresponding values of `rv_guess` listed in GALAH DR3. The mean radial velocity listed in Gaia DR2 is also given, with its formal error and the number of epoch transits over which it has been computed.

	Asiago 1.82m Echelle			GALAH DR3			Gaia DR2		
	UT middle	RV _☉ (km/s)	err (km/s)	UT middle	RV _☉ (km/s)	err (km/s)	<RV _☉ > (km/s)	err (km/s)	N
GaSS 1-9	2020-07-04 22:30	-130.06	0.51	2017-04-09 17:56	-131.58	0.41	-133.07	0.60	13
	2020-10-03 17:49	-131.04	0.15						
GaSS 1-12	2019-09-11 19:13	61.11	0.48	2017-06-04 15:59	51.88				
	2020-07-05 23:15	56.22	0.21						
	2020-10-03 18:10	54.57	0.40						
GaSS 1-13	2020-07-04 22:54	-362.31	1.23	2014-06-11 16:08	-375.27	0.50	-374.54	1.54	4
	2020-10-03 18:51	-373.54	0.18						
	2020-10-29 17:13	-375.50	0.26						
GaSS 1-14	2020-10-03 20:04	-247.37	0.19	2016-08-13 12:56	-247.79	0.40	-250.47	0.61	10
	2020-10-29 17:55	-248.79	0.12						
GaSS 1-15	2020-09-03 21:21	46.40	0.29	2017-09-06 12:14	49.94	0.29			
	2020-10-03 19:47	51.08	0.04						
	2020-10-29 18:15	51.34	0.10						
GaSS 1-20	2020-07-05 21:03	12.95	0.48	2017-06-03 13:27	44.76	0.43	9.36	0.82	10
GaSS 1-21	2020-07-05 20:42	-182.39	1.70	2015-04-29 13:47	-182.82	0.47	-182.22	0.59	9
GaSS 1-23	2020-07-05 21:45	-166.89	0.92	2016-08-16 09:36	-167.23	0.45	-169.53	1.01	10
GaSS 1-31	2020-07-05 23:36	69.59	0.15	2017-11-06 10:00	70.13	0.51	68.02	0.82	7
	2020-10-03 18:27	70.92	0.16						
	2020-10-17 18:20	68.72	0.72						
GaSS 1-33	2020-10-03 19:10	-206.97	0.36	2014-07-08 17:31	-205.14				
	2020-10-29 18:54	-206.10	1.05						

at U -band wavelengths, badly affected the study of flickering, with rarer attempts carried out (e.g. [Dobrzycka, Kenyon, & Milone 1996](#); [Sokoloski, Bildsten, & Ho 2001](#); [Gromadzki et al. 2006](#); [Zamanov et al. 2011](#)). To further complicate the matter, the sensitivity of CCDs, that extends up and beyond $1 \mu\text{m}$, allows signal to be recorded from the red-leak affecting most U filters, especially those of the modern multi-layer dielectric type. Such a red-leak may be so severe in the case of cool giants, that the fraction of recorded photons coming through the red-leak easily outnumber those going through the proper transmission profile of the U -band ([Munari & Moretti 2012](#)).

To search for flickering among our candidate *acc*-SySt we used a 50cm telescope, with a 40arcmin well corrected field of view and quality photometric filters, operated robotically for ANS Collaboration in Chile at San Pedro de Atacama. For the above described limitations about U filters, we selected to search for flickering in B -band, with interspersed observations in V -band serving to construct the $B-V$ colour base for the transformation from the instantaneous local photometric system to the Landolt's standard one. Local photometric sequences were extracted from the APASS multi-epoch, all-sky *BVgri* photometric survey ([Henden et al. 2016](#)) in its DR8 version.

Given the much brighter emission of the M giant in B compared to U , the expected amplitude of observable flickering decreases to (at most) a few hundredths of a magnitude. To be detected, such a tiny amount of variation requires highly accurate observations and careful data reduction, under clear and stable skies as usually enjoyable in Atacama. We adopted integration times in B of 30sec for the brightest targets and 5min for the faintest, with 60sec for the bulk of objects, thus ensuing that all objects have been observed at

high S/N (>100 on each single point) while remaining short of the saturation thresholds and non-linear regime. Every 10 exposures in B , one was obtained in V to compute the coefficients of the transformation colour equations. The procedure was repeated identically for 70min for each program star. The photometry was performed for most objects in aperture mode, their high galactic latitudes implying sparsely populated fields and therefore no need to revert to PSF-fitting, which was instead necessary for three targets. On average, the 50 field stars closest on the image to the symbiotic star, of a similar magnitude and well isolated from neighboring stars were also measured on all recorded images in exactly the same way as the symbiotic star. The photometry of these 50 field stars was then inspected looking for those with a $B-V$ colour as close as possible to the symbiotic star in the center. Typically 5 such stars were found, with a few cases scoring just 2 and others up to 8. These field stars with magnitude and colour closely matching those of the symbiotic star, serve as samplers of the observational noise above which the flickering has to be detected: the closely similar colour nulls the effects of differential atmospheric transmission, and the closely similar brightness nulls the non-linear effects in the differential statistical noise.

The program *acc*-SySt subjected to the search for flickering are listed in Table A4, together with the HJD of the central image for the 70min time series, and the average of B and V measured magnitudes during such time series. The error of such B and V data is totally negligible in its Poissonian component, while the amount due to transformation from the local system to the APASS one (closely adherent to Landolt's) is systematic and constant for a given object and amounts on average to 0.008 mag (which obviously cancels out when comparing flickering data within a given time-series).

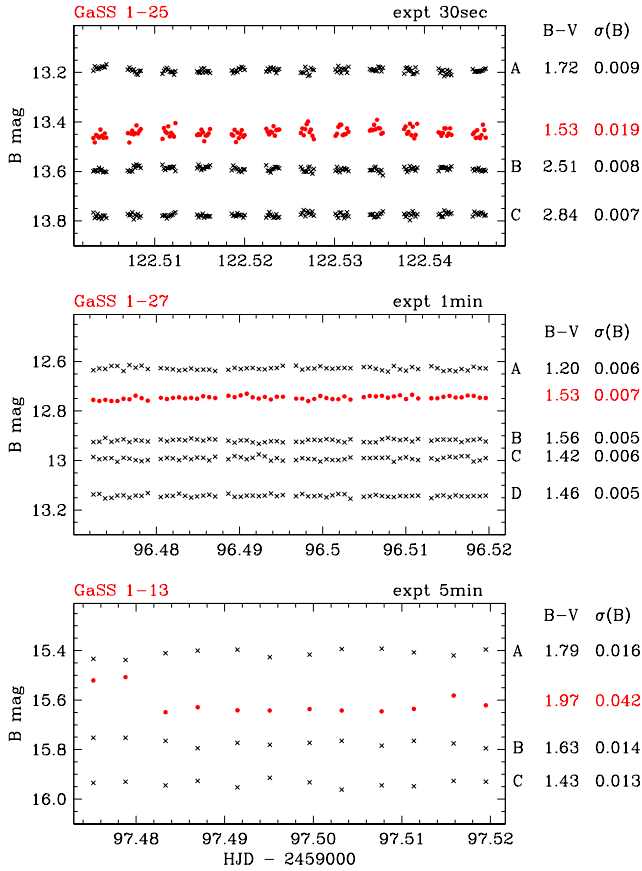


Figure 10. Examples of the B -band time series collected on the program stars, with 30sec, 1min and 5min sampling time (from top to bottom), in search for flickering from the accretion disk. The regular gaps correspond to the acquisition of V -band frames for the calibration of colour equations to transform data to the standard Landolt system. The measured $B-V$ colour of the symbiotic star (in red and filled circles) and of nearby field stars of similar brightness and colour (in black and crosses), is marked to the right, together with the dispersion around the median of the plotted B -band data. Symbiotic stars on the top and bottom panels clearly show flickering well in excess of the noise affecting field stars, while that on the center panel is constant at the same noise level of the field stars.

An example of the collected data is presented in Fig. 10, with one object each for the 30sec, 1min and 5min sample times. At the top and bottom panels we show objects with a clear detection of flickering well in excess of the noise affecting the field stars as usually quantified by their respective rms deviation from the mean (Dobrzycka, Kenyon, & Milone 1996), while in the center we present a non-flickering symbiotic that remains stable at a few millimag-level through the 70min monitoring. GaSS 1-25 at the top of Fig. 10 exemplifies the frequent case of incessant flickering (e.g. RS Oph as observed by Dobrzycka, Kenyon, & Milone 1996), while the behavior displayed by GaSS 1-13 at the bottom of Fig. 10, i.e. isolated flarings over an otherwise relative flat background, is a close match to that observed by Zamanov et al. (2017) in EF Aql.

The objects for which flickering was detected well above observational noise are marked with an ‘F’ in the ‘Flk’ column of Table 5. The detectability of flickering and its amplitude are usually dependent on the actual epoch of observation (Stoyanov et al. 2018). Orbital phases with the hot spot in plain view are favoured (WD at quadrature moving toward superior conjunction), while others can be detrimental, e.g. during eclipses or passage at apostron in a

highly eccentric orbit (with consequent reduction in mass transfer rate). Therefore, stars in Table 5 that failed to show flickering at the single epoch of our observation could do otherwise at a later revisit. This is also the case for SU Lyn. When it was observed in late 2015 by Mk16 it was in a high accretion state and it flickered wildly, while it was in a low accretion state and did not flicker when Dimitrov et al. (2018) performed their observations in January 2018. Similarly, while large amplitude flickering has always been the rule for MWC 560 (eg. Lucy et al. 2020), it has disappeared altogether during the last couple of years (Zamanov et al. 2019).

We postpone a detailed analysis of the data collected during our search for flickering for the program stars to a follow-up paper. Derivation of temperature and radius of the region(s) responsible for the observed flickering (e.g. Zamanov et al. 2020) is straightforward but largely out of the goals of this paper, as it is the search about possible quasi-periodicities or signatures of the WD rotation (e.g. Sokolowski & Bildsten 1999; Zhekov & Tomov 2019). Such analysis will strongly benefit from further observations we have planned for the SySt reported in this paper and are carrying out also for other SySt assigned to later papers in this series.

5.5 Satellite X-ray/UV observations

The presence and nature of the accreting source in *acc*-SySt systems, either a WD or a NS, is best defined by satellite observations performed in the ultraviolet and X-rays, where the peak of the emissivity for accretion-induced processes is located (e.g. Masetti et al. 2007a and references therein, and also Kuranov & Postnov 2015 for a recent review). The X-ray/UV properties of the *acc*-SySt prototype SU Lyn have been investigated by Mk16, Lopes de Oliveira et al. (2018), and Kumar et al. (2021) based on observations with *Swift*, *NuSTAR* and *ASTROSAT* satellites. They found SU Lyn to show (i) a large (by a factor of a few hundred in flux) UV excess with respect to a ‘normal’ red giant; (ii) long-term (months to years) hard X-ray variations by an order of magnitude between low- and high-level states in the 15–35 keV hard X-ray emission; and (iii) fast UV variability during the high X-ray states (flickering). In the latter ones, the average X-ray flux was $\sim 10^{-11}$ erg cm $^{-2}$ s $^{-1}$ in the 0.3–50 keV band, with the spectrum modelled with a thermal plasma of temperature $kT \sim 20$ keV, plus a fluorescent iron emission at 6.4 keV, absorbed by a hydrogen column N_H as large as $\sim 3 \times 10^{22}$ erg cm $^{-2}$. This absorption has however little effect on the UV excess observed from this source. At a distance of 650 pc, this corresponds to unabsorbed X-ray luminosities of up to $\sim 10^{33}$ erg s $^{-1}$ in the high state, and a factor of 10 larger in the UV. The passage from low- to high-level states in the UV and X-ray emission is attributed to large excursions in the transfer and accretion rates.

In anticipation of a devoted observing campaign, we have performed some quick exploratory observations of three of the *acc*-SySt discovered in this paper with the *Swift* satellite (Gehrels et al. 2004), and for comparison of three of the identified radial pulsators considered as a control sample. The observations have been carried out in Target-of-Opportunity mode. This type of observations is generally limited to roughly 2000 seconds per object, so this can be considered as a quick and rather shallow survey of our target sample. The pointings were performed in two time slots: the first one in September–October 2019, and the second one in June 2020. The results are summarized in Table 7.

Our *Swift* observations were acquired with the on-board instruments X-Ray Telescope (hereafter XRT, Burrows et al. 2005) and UltraViolet–Optical Telescope (hereafter UVOT, Roming et al.

Table 7. Results of the *Swift* XRT and UVOT observations of some of the *acc*-SySt presented in this paper. The fluxes are in units of 10^{-13} erg cm $^{-2}$ s $^{-1}$. The bottom three objects are radial pulsators observed for comparison. The data for 20 35 04.52 –05 47 35.3 include also additional 485sec exposure obtained on 8 Sep. 2019.

name / RA,DEC	Obs. date	Start time (UT)	XRT obs. duration (s)	0.3–10 keV count rate	0.3–10 keV flux	UVOT obs. duration (s)	UVM2 mag.
GaSS 1-11	13 Jun. 2020	12:05	1885	<3.0e-3	<2.6e-13	1864	17.33±0.06
GaSS 1-12	16 Sep. 2019	00:02	1516	<3.2e-3	<2.8e-13	1701	16.21±0.04
GaSS 1-31	14 Jun. 2020	01:01	839	<3.7e-3	<3.3e-13	830	>19.92
05 11 30.88 –61 29 03.6	10 Jun. 2020	06:31	1973	<1.7e-3	<1.5e-13	1948	>20.65
20 06 56.32 –28 35 32.3	11 Oct. 2019	00:49	1536	<2.5e-3	<2.2e-13	1527	>20.71
20 35 04.52 –05 47 35.3	04 Sep. 2019	12:23	1504	<3.6e-3	<3.2e-13	1485	>20.82

2005). The XRT allows covering the X-ray band between 0.3 and 10 keV band, whereas UVOT data were collected using the UV filter *UVM2* (reference wavelength: 2246 Å; see Poole et al. 2008 and Breeveld et al. 2011 for details). On-source pointings were simultaneously performed with the two instruments and lasted between ~800 and ~2000 s.

All observations were reduced within the *FTOOLS* environment (Blackburn 1995). The XRT data analysis was performed using the *XRTDAS* standard pipeline package (*XRTPIPELINE* v. 0.13.4) in order to produce screened event files. All X-ray data were acquired in photon counting (PC) mode (Hill et al. 2004) adopting the standard grade filtering (0-12 for PC) according to the XRT nomenclature. For each source, scientific data were extracted from the images using an extraction radius of 47'' (20 pixels) centered at the optical coordinates of the source, while the corresponding background was evaluated in a source-free region of radius 94'' (40 pixels) within the same XRT acquisition. In all cases, no emission above a signal-to-noise threshold $S/N = 3$ was detected. The XRT count rate upper limits in the 0.3–10 keV range were then measured within the *XSPEC* package.

X-ray flux limits were determined using the *WEBPIMMS* online tool³ by assuming a spectral model similar to that of Mk16 for SU Lyn, i.e. a thermal plasma emission with temperature $kT = 17$ keV absorbed by a column density $N_H = 2.9 \times 10^{22}$ cm $^{-2}$, which implies a count rate-to-flux conversion factor of $\sim 8.8 \times 10^{-11}$ erg cm $^{-2}$ s $^{-1}$ cts $^{-1}$. We note that, with this model, the unabsorbed fluxes (in Table 8) in this same band are about 50% larger than the absorbed ones.

Count rates on Level 2 (i.e. calibrated and containing astrometric information) UVOT images at the position of the objects of our sample were measured through aperture photometry using 5'' apertures, whereas the corresponding background was evaluated for each image using a combination of several circular regions in source-free nearby areas. Magnitudes and upper limits were measured with the *UVOTSOURCE* task. The data were then calibrated using the UVOT photometric system described by Poole et al. (2008), and we included the recent (November 2020) fixings recommended by the UVOT team.

Of the three *acc*-SySt observed with *Swift*, two were found to be strong UV emitters, confirming their symbiotic nature. The third, GaSS 1-31 was not detected. There may be a clear reason for

that, though. The *Swift* pointing was carried out on 14 June 2020. Three weeks later, on 5 July 2020, we observed the same star with the Asiago 1.82m and the Echelle spectrograph. The $H\alpha$ profile for that date is presented in Fig. 9, and doesn't show the faintest trace of an emission. In addition, the equivalent width of the $H\alpha$ absorption is same as for field stars of the same spectral type (and greater than for the other dates in Fig. 9), indicating no partial filling from even very faint emission. In short, it looks like the emission from the accretion disk was 'switched-off' at the time of the *Swift* pointing, with consequent non-detection. An eclipse behind the M-giant seems improbable in view of the limited variability of the epoch GALAH and Asiago radial velocities listed in Table 6 (and their similarity with the average velocity provided by Gaia DR2), precluding a high orbital inclination for GaSS 1-31. It rather seems a drastic reduction in the mass accretion rate was taking place at the time of *Swift* observations. This could have been caused by a reduction in the wind blown-off by the M giant or passage at apoastron in a highly eccentric orbit. The spectrum taken a hundred days later (that for 3 Oct 2020 in Fig. 9) shows that accretion has weakly resumed, with both a reduction in the equivalent width of $H\alpha$ absorption (partially filled-in) as well as emission wings extending above the local continuum.

None of the three radial pulsators we tried with *Swift* were detected, in spite of having been selected among those showing the strongest $H\alpha$ and $H\beta$ emission on GALAH spectra (far stronger than typically observed in *acc*-SySt). This supports the clear-cut role of satellite UV observations in segregating *acc*-SySt (Sahai et al. 2015), in particular from radial pulsators of similar spectral appearance on optical spectra.

A few final words are in order to explain the non-detection of GaSS 1-11 and 1-12 in X-rays in our shallow observations. The upper limit to their flux is about 0.01× the flux Mk16 recorded from SU Lyn during their *Swift* observations. Those observations of SU Lyn were obtained during an exceptionally bright state of the accretion disk (cf. Fig. 2 and the discussion at the end of Section 3), while the flux at other times (when the $H\alpha$ shown by SU Lyn is much weaker and more similar in appearance to that revealed by GALAH spectra for our sample of 33 *acc*-SySt) was just 1/10 of that (cf. Lopes de Oliveira et al. 2018). There are two other factors playing against GaSS 1-11 and 1-12. The most important is the distance. SU Lyn is just 0.65 kpc away, while GaSS 1-11 and 1-12 are respectively at 6.6 and 4.6 kpc distance according to Gaia *eDR3* parallaxes, corresponding to dilution factors of 100 and 50. In addition, SU Lyn is seen face-on, while the unknown orbital

³ <https://heasarc.gsfc.nasa.gov/cgi-bin/Tools/w3pimms/w3pimms.pl>

Table 8. Unabsorbed accretion luminosity from the *Swift* data in Table 7 (see Section 5.6 for details).

symbiotic star	L_{UV} (erg s^{-1})	L_{UV} (L_{\odot})	M_{acc} ($M_{\odot} \text{ yr}^{-1}$)
GaSS 1-11	1.43e34	3.7	1.7e-9
GaSS 1-12	3.30e34	8.5	4.0e-9
GaSS 1-31	<4.29e32	<0.11	<5.1e-11

Table 9. Flux recorded in $H\alpha$ and corrected for reddening ($F(H\alpha)$), isotropic luminosity radiated in $H\alpha$ at Gaia *e*DR3 parallax ($L(H\alpha)$), and accretion luminosity (L_{acc}) derived as described in Section 5.6 for the program star with available Asiago spectra to flux-calibrate GALAH spectra.

symbiotic star	$F(H\alpha)$ ($\text{erg cm}^{-2} \text{ s}^{-1}$)	$L(H\alpha)$ (erg s^{-1})	L_{acc} (L_{\odot})
GaSS 1-12	1.391E-13	3.52e+32	14
GaSS 1-14	3.307E-14	2.93e+32	12
GaSS 1-15	3.205E-14	3.23e+31	1
GaSS 1-23	7.257E-14	2.00e+32	8
GaSS 1-25	1.179E-13	2.61e+32	10
GaSS 1-28	2.785E-14	1.88e+32	7
GaSS 1-31	2.367E-13	5.24e+32	22

inclination of GaSS 1-11 and 1-12 introduces a reduction in flux proportional to $\cos i$ and a further reduction for limb-darkening reasons. Considering all factors together, it is no wonder that GaSS 1-11 and 1-12 fell below the X-ray detection threshold of snapshot ToO with *Swift*.

5.6 Accretion luminosities

We have previously stated that the aim of the present paper is to search for new SySt accreting at low rates similar to SU Lyn. Mass accretion rate (M_{acc}) and accretion luminosity (L_{acc}) are related by the usual

$$L_{\text{acc}} = G \frac{M_* M_{\text{acc}}}{R_*} \quad (4)$$

where M_* and R_* are the mass and radius of the accreting object, respectively. The accretion on a WD, as it is the case for SU Lyn, radiates most of its output in the UV and much less into X-rays, while the reverse applies to neutron stars and their much deeper potential well.

The UVM2 magnitudes of the new SySt in Table 7 correspond to flux densities (in units of $10^{-15} \text{ erg cm}^{-2} \text{ s}^{-1} \text{ \AA}^{-1}$) of 0.54, 1.52 and <0.05 , for GaSS 1-11, 1-12 and 1-31, respectively (from the countrate-to-flux calibration given in Poole et al. 2008 and Breeveld et al. 2011). Then, considering the distances and $E(B-V)$ colour excesses reported in Table 5, correcting for the Galactic reddening according to the prescription in section 3.2 of Kataoka et al. (2008) and the UV correction coefficients in their table 5, and assuming for the three objects a flat spectral distribution in the UV as Mk16 did for SU Lyn, we obtain the unabsorbed UV luminosities listed in Table 8. In the hypothesis of accretion onto a WD of mass

$1 M_{\odot}$, as Mk16 has inferred for SU Lyn, in Table 8 we report also the corresponding accretion rates.

For the other new SySt that were not observed by *Swift*, an estimate of L_{acc} can be derived from the flux recorded in the $H\alpha$ emission. If an emission line forms in an accretion disk, the flux radiated by the line and the flux emitted by the disk as a whole are related. The correlation can be tight, with temporal variations in L_{acc} that may be accurately tracked and replicated by $L(H\alpha)$ (cf. Munari et al. 2019, their fig. 14).

GALAH spectra are unfortunately not flux-calibrated. To circumvent the problem, we look for assistance from the fluxed Asiago spectra. After de-reddening the Asiago spectra for the E_{B-V} values listed in Table 5, we used them to flux-calibrate the GALAH spectra of the corresponding objects. Being primarily interested in deriving just an order-of-magnitude, and noting the new SySt exhibit only a limited photometric variability (cf. Section 4.6 above), we ignore the fact that Asiago and Galah spectra are not simultaneous. On the template-subtracted version of the flux-calibrated GALAH spectra, we measured the integrated flux of $H\alpha$ emission line $F(H\alpha)$ (therefore already corrected for reddening), and list it in Table 9, where we consider only the new SySt with Gaia *e*DR3 distances in Table 5. If d is the distance, the luminosity $L(H\alpha)$ radiated isotropically by the disk in $H\alpha$ is obviously

$$L(H\alpha) = 4\pi d^2 F(H\alpha) \quad (5)$$

As customary practice, we may write a power-law proportionality between the luminosity radiated in the line and by the disk as a whole:

$$\log(L_{\text{acc}}) = \alpha_{H\alpha} + \beta_{H\alpha} \times \log(L(H\alpha)) \quad (6)$$

where $\alpha_{H\alpha}$ and $\beta_{H\alpha}$ are coefficients specific to $H\alpha$. Adopting their value from Mendigutía et al. (2011), we have derived the L_{acc} listed in the last column of Table 9. The accretion luminosities derived directly from *Swift* ultraviolet data or estimated from the flux radiated in $H\alpha$ are similar, and confined to the 1–20 L_{\odot} range, the same roughly spanned by SU Lyn while varying between high- and low-states. Interestingly, there is an estimate of L_{acc} for GaSS 1-12 both from the *Swift* UV observations and also from $H\alpha$ emission line flux, and the two differ by less than a factor of 2. While this can be read as an indirect confirmation of the reliability of L_{acc} estimated from $H\alpha$, it also points to the constant variability of L_{acc} observed in *acc*-SySt. In fact, the $F(H\alpha)$ of GaSS 1-12, measured on the fluxed version of the Echelle spectra presented in Fig. 9, varies by more than the above $2\times$ factor.

5.7 Orbital-like periodicities

The long-term lightcurves of SySt are usually reconstructed from multi-band photometric campaigns (e.g. Skopal et al. 2007, 2012; Sekeráš et al. 2019), from digging historical plate archives (e.g. Munari & Jurdana-Šepić 2002), or searching the public databases of all-sky patrol surveys (e.g. Gromadzki et al. 2009; Gromadzki, Mikołajewska, & Soszyński 2013; Munari et al. 2021). Aside from the obvious effect of eclipses for systems seen at high inclination, the orbital motion may affect also the lightcurve of SySt seen at intermediate inclinations. The basic type of orbital-induced modulation of the lightcurve of non-eclipsing SySt is shown in Fig. 11 (adapted from Munari 2019), aiming to highlight the interplay between the irradiation effect (better visible in the bluest photometric bands and for *burn*-SySt) and the ellipsoidal distortion (which is more prominent in the reddest bands and in *acc*-SySt).

We have already mentioned that the M3III giant of T CrB fills

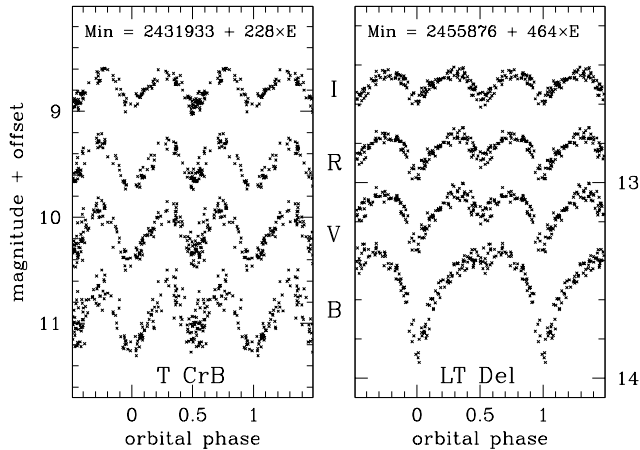


Figure 11. Examples of the modulation of the *BVRI* lightcurves induced by orbital motion in non-eclipsing symbiotic stars (see Section 5.7). Note the increasing impact of flickering going toward bluer bands for the accreting-only T CrB, and its absence for the burning-type LT Del. The lightcurves of both objects are obtained from data extending over at least 10 consecutive orbital cycles. Adapted from Munari et al. (2019).

its Roche lobe, causing an ellipsoidal deformation of the surface, that along an orbital period presents to observers twice the larger projected area (the two maxima in the lightcurve) and twice the smaller one (the two minima). The reason for the change in brightness is primarily geometric, so its shape is similar at all wavelengths as the left panel of Fig. 11 shows. In that figure, the presence of flickering superimposed to the regular orbital motion is quite obvious, in the form of a scatter of points of an increasing amplitude moving from redder to bluer bands (cf. Section 5.4 above). A search for periodicity on such a lightcurve would return *half* the value of the true period: 114 days instead of 228. It is the spectroscopic orbit that would solve the uncertainty in favor of 228 days.

The cool giant in LT Del, the other symbiotic star in Fig. 11, equally fills its Roche lobe, but contrary to T CrB, its WD is burning on its surface. The hot and bright companion irradiates the facing side of the cool giant, thus heating its photosphere and partially ionizing the atmosphere above it, with the consequence to make the system brighter when the irradiated side is in full view (Kenyon 1986). The effect is larger going to bluer wavelengths. Thus, while the behavior of T CrB and LT Del is the same in *I*-band where the ellipsoidal distortion of the cool giant dominates, differences begin to emerge moving toward shorter wavelengths: the irradiation effect takes the lead in shaping the *B*-band lightcurve of LT Del. If the support of radial velocities is required for T CrB, the orbital period of LT Del can be fixed without uncertainty on the base of multi-band photometry alone. Unfortunately, most all-sky patrol surveys observe in just one band, and a disentangling like that for LT Del is not possible with their data alone, leaving on the desk the ambiguity between P and $2\times P$ for the true orbital period.

We have searched the ASAS-SN photometric data for the 33 candidate *acc*-SySt looking for a type of lightcurve modulation that could be orbitally induced along the lines just outlined for T CrB and LT Del in Fig. 11. We found a suitable shape for 12 of them, and they are presented in Fig. 12, with the corresponding periods listed in Table 5. Their length is rather typical for symbiotic stars, the majority of known cases going from 7 months to 2.5 years (Mikolajewska 2003).

In two cases, GaSS 1-27 and GaSS 1-28, a slight difference in the depth of minima seems enough to resolve the ambiguity between

P and $2\times P$. Given the limited time span of ASAS-SN coverage, such a difference could also result from other causes for photometric variability, and needs confirmation over more orbital cycles. Even more so for a possible third case for unequal minima, that of GaSS 1-33, and its sparsely covered lightcurve (cf Fig. 12). A borderline case is that of GaSS 1-8, with just a hint of a secondary minimum around phase 0.5 which could be spurious. The modulation displayed by GaSS 1-28, while somewhat larger than usual, is a fine match in both shape and amplitude to that of Hen 3-1591, whose modulation Gromadzki et al. (2007) attribute to orbital modulation and report that it is confirmed by variations in radial velocity.

The remaining objects in Fig. 12 show equal-depth minima, so the actual orbital period could be twice the value listed in Table 5 and on the ephemerides in their respective panels of Fig. 12. To help resolve the controversy, we have started a *BVRI* monitoring of them all, but the fruits of this effort will be collected only in a few years time, when at least a few orbital cycles will be covered.

5.8 Lithium

Wallerstein et al. (2008), in their chemical analysis of high resolution spectra of M giants in symbiotic stars, found that the recurrent novae and accreting-only systems T CrB and RS Oph show an over-abundance of ${}^7\text{Li}$ in their spectra. None of the other symbiotic stars in their large sample showed ${}^7\text{Li}$ enhancement and none was known to have undergone nova outbursts similar to T CrB and RS Oph. The over-abundance of ${}^7\text{Li}$ in T CrB has been recently revised upward to $A(\text{Li}) = 2.4 \pm 0.1$ by Woodward et al. (2020). The apparent link between ${}^7\text{Li}$ and nova outbursts has been further reinforced when the symbiotic star V407 Cyg erupted in 2010. ${}^7\text{Li}$ over-abundance was discovered earlier in V407 Cyg by Tatarnikova et al. (2003) at a time when the object was simply known as a Mira variable with a possible companion, and therefore attributed to indigenous production via the Cameron & Fowler (1971) mechanism activated in the Mira variable. We know now that also V407 Cyg undergoes nova outbursts, and this sheds an alternative explanation for its ${}^7\text{Li}$ overabundance.

The production of ${}^7\text{Li}$ during nova eruptions has been predicted theoretically (e.g. José & Hernanz 1998; Rukeya et al. 2017; Starrfield et al. 2020) and confirmed observationally (e.g. Tajitsu et al. 2015; Izzo et al. 2015; Molaro et al. 2016). Up to $\sim 1 \times 10^{-5}$ of the whole mass of the ejecta can be in the form of ${}^7\text{Li}$, actually ${}^7\text{Be}$ that will decay into ${}^7\text{Li}$. The large amounts produced during outbursts (especially those occurring on white dwarfs of the Carbon-Oxygen type), suggests that novae could be the main producer of ${}^7\text{Li}$ in the Milky Way (Molaro et al. 2020).

It is tempting to attribute the over-abundance of ${}^7\text{Li}$ observed in T CrB, RS Oph and V407 Cyg to pollution of the cool giant by the ejecta of the nova outbursts experienced by the WD companion. Their eruptions occur at a high frequency (eight have been observed in historic times for RS Oph) such that they could replenish the surface of the cool giant with ${}^7\text{Li}$ faster than convection can dilute ${}^7\text{Li}$ into the interior of the star. Alternatively, ${}^7\text{Li}$ could instead come from the interior of the cool giant, and conditions leading to an efficient transport of ${}^7\text{Li}$ to the surface could also lead more probably to nova outbursts as a consequence of a higher mass loss rate and/or an enrichment in CNO nuclei.

In analogy with T CrB, RS Oph and V407 Cyg, we have searched for ${}^7\text{Li}$ overabundance in our 33 candidate new SySt by comparing with the template spectrum for their *f*-ratio, and found a clear case of enhancement in GaSS 1-26, as shown in Fig. 13. The object is completely anonymous (no matching entry in SIMBAD,

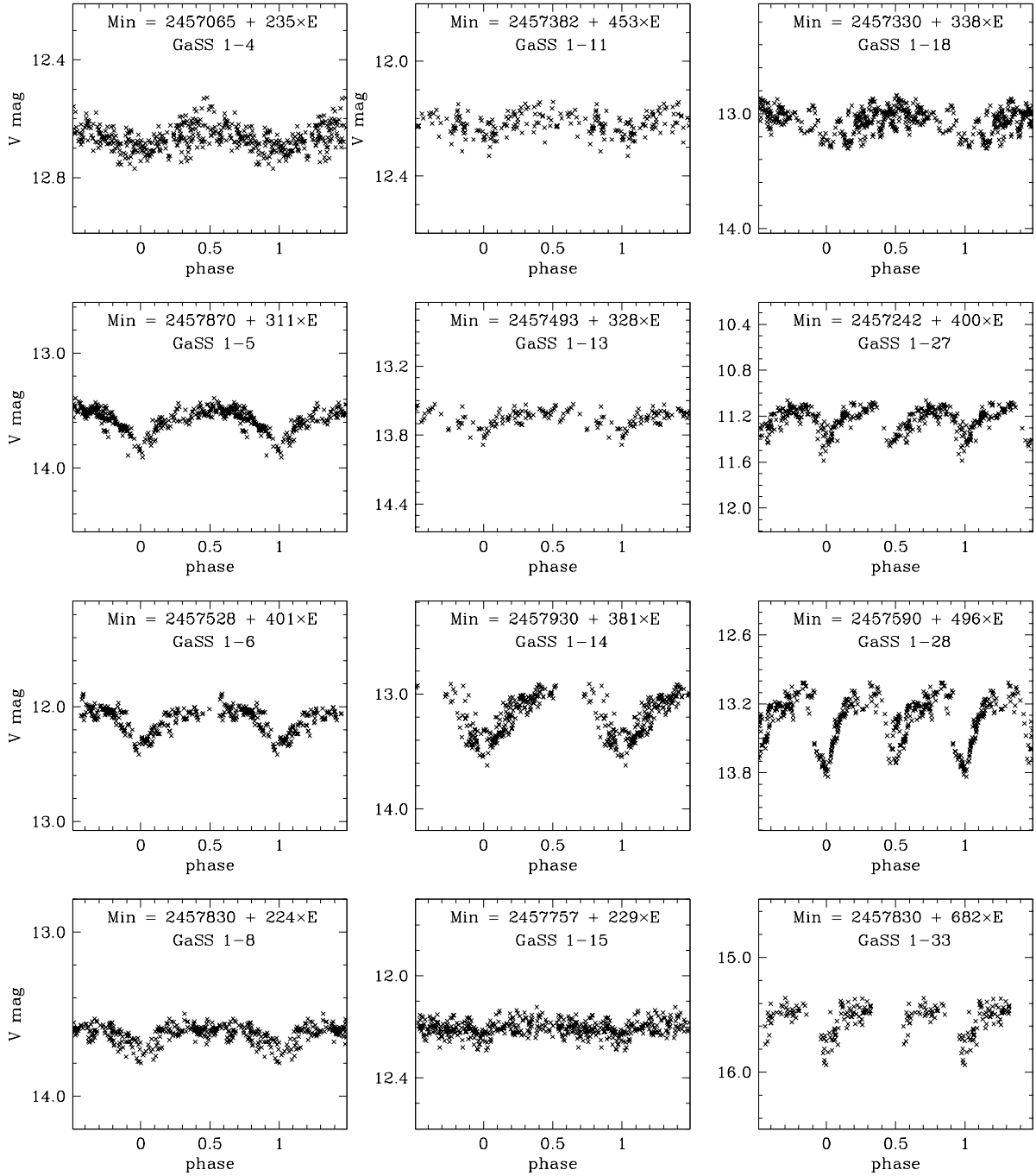


Figure 12. Phased light-curves (see ephemeris at the top of each panel) for the twelve *acc*-SySt marked in Table 5 as showing a modulation reminiscent of orbital motion.

VSX and similar catalogs) and its optical variability is inconspicuous (cf Fig. A7 in the Appendix).

We have subjected GaSS 1-26 to a search for flickering and got a robust detection (cf Table 5), which supports its binary nature and the presence of an accreting companion in the form of a WD.

Armed with that, we turned to the Harvard plate stack in search for an unnoticed nova outburst in the distant past. DASCH project provides access to calibrated scans of the huge collection of sky patrol photographic plates obtained over a century with Harvard astrographs located in both hemispheres (Grindlay et al. 2009). The area of the sky where GaSS 1-26 is located has not yet been included

in the available DASCH data releases (1 to 6). We have been however granted access to the data for the area of sky around GaSS 1-26 prior to their publication in DASCH DR7, currently planned for July 2021. This led to some initial excitement when two plates for June 6, 1908 and September 17, 1916 were logged as reporting GaSS 1-26 much brighter than at other epochs and at a blue magnitude compatible with a nova outburst. This pair of observations belongs to a time interval with very few Harvard plates covering the GaSS 1-26 position and being deep enough to have recorded it in quiescence (we measured it at $B=15.4$ during our search for flickering, cf. Table A4, thus quite faint for the photographic means of the time).

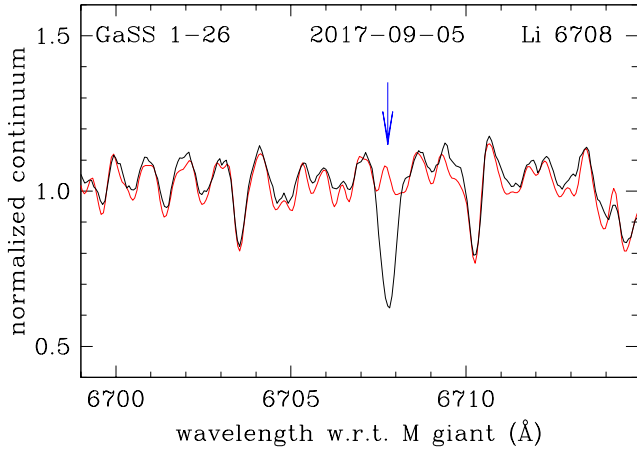


Figure 13. The GALAH spectrum of GaSS 1-26 (black) around the position of LiI 6707.8 Å compared with that (red) of the template for the same f -ratio bin. The overabundance of LiI is quite obvious.

To assess if any nova outburst had really affected GaSS 1-26 in 1908 and/or 1916, we asked for and were provided with a scan of both plates (Edward Los, private communication). Inspection of these scans reveals the presence of artefacts at the astrometric position for GaSS 1-26, in the form of ink from a pen marking for the 1908 plate and a scratch on the emulsion for the 1916 one. Therefore, no nova outburst affected GaSS 1-26 in either 1908 and 1916. Even if the search on Harvard plates for unnoticed past nova outbursts has not been fruitful, it should be extended to other photographic plate archives, although not many cover the southern hemisphere at faint magnitudes and over protracted periods of times, and even less have preserved the plates in good conditions and provide access to them in person or via digitized scans.

In favor of a possible pollution scenario for the ${}^7\text{Li}$ in GaSS 1-26 is the fact that indigenous ${}^7\text{Li}$ production via the Cameron & Fowler (1971) mechanism is expected to occur during hot-bottom burning conditions (HBB), when the outer part of the burning H-shell is included in the envelope convection. A key aspect of HBB is the existence of a lower mass limit for it to occur, which depends on metallicity (Herwig 2005). The minimum initial mass for HBB is $M_{\text{ini}} \geq 5 M_{\odot}$ at solar metallicity (Forestini & Charbonnel 1997), which can decrease down to $3 M_{\odot}$ for very metal-poor stars (Siess, Livio, & Lattanzio 2002). The latter is obviously not the case given the otherwise normal spectrum displayed by GaSS 1-26. The faintness and negligible reddening place GaSS 1-26 at a great distance from us; its Gaia $e\text{DR3}$ parallax is affected by a large error, but it seems safe to argue that a lower limit to the distance is 10 kpc. At a galactic latitude $-10^{\circ}6$, it means a height over the galactic plane of $z \geq 1.9$ kpc. It would be rather atypical to find a young and massive $M_{\text{ini}} \geq 5 M_{\odot}$ star at such a large height above the Galactic plane.

5.9 Evolutionary status

The nature of the new SySt will be investigated in detail elsewhere, including their chemical partition and Galactic orbits. However, some preliminary comments seem in order here.

To assess the evolutionary status of the new SySt, we have taken their JHK_S near-IR photometry from 2MASS survey (Cutri et al. 2003) and after correcting for reddening and distance given in Ta-

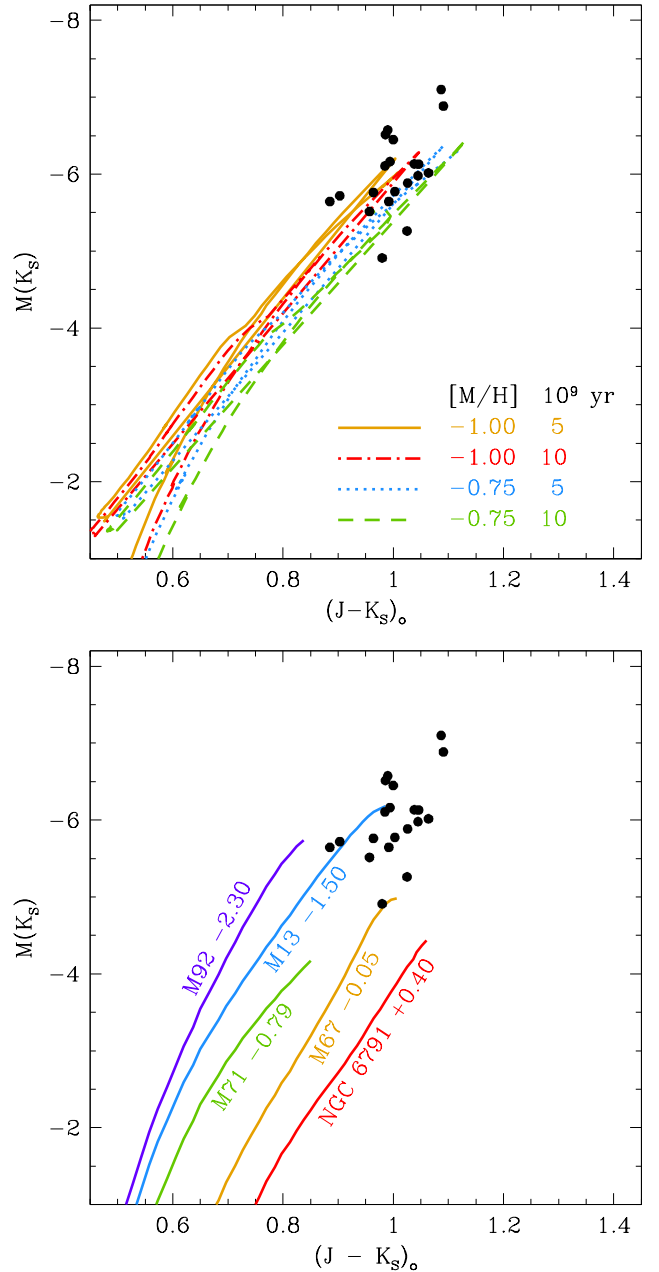


Figure 14. Location of the new SySt on the near-IR isochrone plane, compared with Padova PARSEC isochrones (top) and observed ones (bottom) for clusters spanning a range in metallicity (see Section 5.9 for details).

ble 5, we have plotted their positions on the absolute $M(K_S)$ /de-reddened $(J - K_S)_0$ plane in Fig. 14.

On the top panel of Fig. 14, the comparison is carried out against the Padova PARSEC isochrones (Bressan et al. 2012; Marigo et al. 2017; Pastorelli et al. 2020). It provides evidence that the new SySt are all located close to the tip of the Giant Branch, and that they are relatively old and metal poor objects. This conforms with their significant height z above the Galactic plane as given in Table A2. For that age and metallicity, their mass estimated from the isochrones ranges from 1.03 to $1.22 M_{\odot}$. Similar conclusions are drawn by comparison with the observed isochrones compiled by Karaali, Bilir, & Gökçe (2013) for a sample of clusters spanning

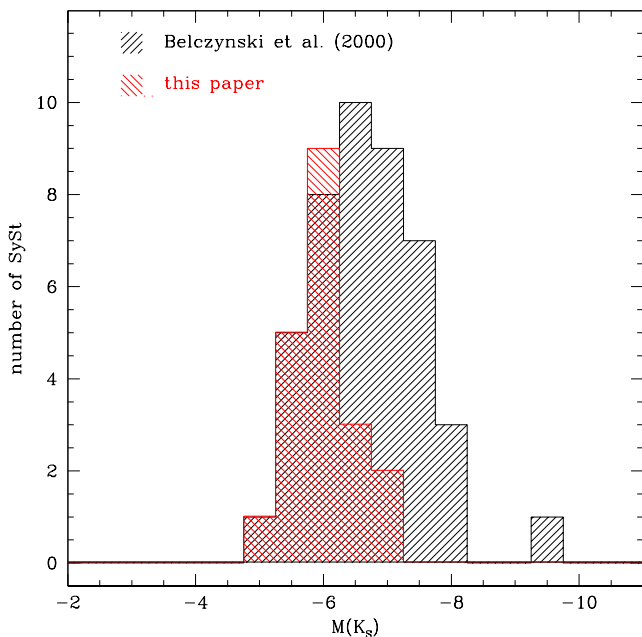


Figure 15. Distribution in absolute 2MASS K_S magnitude of Belczyński et al. (2000) symbiotic stars with an M spectral type, and those from the present paper. Only objects with a Gaia $eDR3$ parallax satisfying the accuracy condition $\sigma(\pi)/\pi < 0.2$ are plotted.

a large range of observed metallicities, as illustrated in the bottom panel of Fig. 14.

How do the red giants of the new SySt compare to well established SySt? This is addressed in Fig. 15, where their distributions in $M(K_S)$ are compared. For the well established SySt we adopted the catalog by Belczyński et al. (2000), and retained only the 44 objects with a giant of M spectral type and with a Gaia $eDR3$ parallax accurate enough to satisfy the inversion condition $\sigma(\pi)/\pi < 0.2$. To compute their $M(K_S)$ we adopted for them the interstellar extinction estimated from the Bayestar 2019 3D model of the Galaxy (Green et al. 2019).

The distribution in Fig. 15 of the new and the well established SySt is the same. The fact that GALAH is a magnitude-limited survey ($12 < V_{JK} < 14$) means that intrinsically brighter objects need to be at larger distances to fall between the limits in magnitude. The lack of GALAH new SySt at the brighter $M(K_S)$ values in Fig. 15 simply reflects the fact that current Gaia $eDR3$ parallaxes are not accurate enough to satisfy the condition $\sigma(\pi)/\pi < 0.2$ for the most distant, and therefore intrinsically brightest objects. It may be guessed that future Gaia data releases will push forward the horizon of parallax accuracy and allow to include the remaining new SySt and let them populate the histogram of Fig. 15.

6 CONCLUSIONS AND FUTURE PROSPECTS

We present the discovery and characterization of 33 bona-fide candidates of the accreting-only type of symbiotic stars. So far, this class of binary systems has evaded a thorough scientific scrutiny, otherwise received by its counterpart, the nuclear-burning class of symbiotic stars. Both describe the same underlying configuration, a binary system composed of a red giant and a degenerate companion, however, they are distinguished by the physical processes under way inside the system and the consequent observational implications, fa-

voring the study of *burn*-SySt. Because *acc*-SySt are believed to be much more abundant in the Galaxy than *burn*-SySt, while the ratio of known (investigated) objects is just the reverse, it is important to uncover this hidden population of interacting binary stars in order to assess the viability of symbiotic stars as progenitors of type Ia supernovae, their impact on the pollution of the ISM, and to better understand the cycle of exchange between the accreting-only and the nuclear-burning phases.

To this end, we have investigated a large sample of 600 255 stars from the GALAH spectroscopic all-sky survey, which, given its unbiased observational strategy, promises to enable the envisaged statistical analysis, while supported by a suite of follow-up observations, provides a rich source of information on individual symbiotic stars. The first 33 candidates presented in this paper were selected using relatively conservative criteria: parallax and colour cut, strength of molecular (TiO) absorption bands, prominence of $H\alpha$ emission line, rejection based on the presence of various observational and reduction artefacts. Furthermore, the photometric light curves were checked to filter out radial pulsators, and great care was taken to reinforce our diagnostics for the symbiotic nature of program stars, building on the knowledge provided by the prototype *acc*-SySt SU Lyn and by conducting follow-up ground and space based observations examining the near-UV excess, RV and emission line variability, optical flickering, and X-ray/UV luminosities.

One of the 33 objects, Gass 1-26, shows a clear enhancement in ${}^7\text{Li}$, which makes it an excellent candidate for follow-up observations aiming to illuminate the possible connection between pollution by novae outbursts and the galactic lithium abundance. Future studies will extend the analysis presented in this work in diverse directions, including:

- weaker emission features in spectra will be considered, as we currently only accept $H\alpha$ profiles which, after subtraction of the template spectrum, reach higher than 0.5 above the adjacent continuum
- other spectral diagnostic features will be established to identify *acc*-SySt despite a possible absence of emission lines, for example a peculiar chemical signature in the spectrum of a giant star that was polluted by eruptions from the compact companion and thus by nuclearly processed material
- earlier spectral types of the primary stars will be investigated, also to account for the more metal-poor systems which do not achieve the same large radius and low surface temperatures as M giants
- automatic and manual inspection of legacy observations is being carried out, such as digging through diverse photometric archives and historical plates stacks in order to find e.g. past active phases or nova outbursts
- existing and future high-energy instruments/surveys (e.g. SWIFT, *e*-ROSITA) can be exploited for follow-up observations or cross-matching of catalogued detections
- combining the chemical abundances and galactic orbits with the aid of the next Gaia releases will provide the means to confirm/reject the belief of symbiotic stars being an old population, primarily belonging to the bulge, thick disk, and halo. This view is built from the infrared characteristics of their cool giants, but it is heavily biased by how (and where in the Galaxy) the classical symbiotic stars were discovered by objective prism surveys of half a century ago. Determining the parent stellar population of symbiotic stars has a profound implication considering that Ia are the only type of supernovae known to erupt in elliptical galaxies, whose stellar populations resemble the bulge of our Galaxy.

The proposed future work will greatly expand the number of characterized *acc*-SySt and thus provide the community with large enough samples for a statistical study of the population of symbiotic stars as a whole. In the meantime, we encourage the readers to further investigate the 33 candidates presented here and help confirm their symbiotic nature with further follow-up observations.

7 DATA AVAILABILITY

The data underlying this article will be shared on reasonable request to the corresponding author.

ACKNOWLEDGEMENTS

This research has made use of the ASI Science Data Center Multi-mission Archive; it also used the NASA Astrophysics Data System Abstract Service, which is operated by the Jet Propulsion Laboratory, California Institute of Technology, under contract with the National Aeronautics and Space Administration. This research has also made extensive use of the SIMBAD and VIZIER databases operated at CDS, Strasbourg, France. We thank Dr. Jamie Kennea and the *Swift* team for the quick approval and the rapid acquisition of the observations we requested. We thank R. Jurdana for the initial contact, and J. Grindlay and E. Los for grating access to DASCH data and scans prior to publication. NM acknowledges financial support through ASI-INAF agreement 2017-14-H.0, and UM through MAINSTREAM - PRIN INAF 2017 "The origin of lithium: a key element in astronomy" (P.I. Paolo Molaro). We would also like to thank S. Dallaporta, G. Cherini and F. Castellani (ANS Collaboration) for contributing to the photometric observations of SU Lyn. This work was supported by the Swedish strategic research programme eSSANCE. G.T. was supported by the project grant "The New Milky Way" from the Knut and Alice Wallenberg foundation and by the grant 2016-03412 from the Swedish Research Council. G.T. acknowledges financial support of the Slovenian Research Agency (research core funding No. P1-0188 and project N1-0040). This research made use of Astropy (<http://www.astropy.org>) a community-developed core Python package for Astronomy (Astropy Collaboration et al. 2013, 2018).

REFERENCES

- Akras S., Guzman-Ramirez L., Leal-Ferreira M. L., Ramos-Larios G., 2019, *ApJS*, 240, 21
- Allen D. A., 1982, *ASSL*, 27. doi:10.1007/978-94-009-7834-8-4
- Allen D. A., 1984, *PASAu*, 5, 369
- Angeloni R., Ferreira Lopes C. E., Masetti N., di Mille F., Pietrukowicz P., Udalski A., Schaefer B. E., et al., 2014, *MNRAS*, 438, 35. doi:10.1093/mnras/stt1823
- Angeloni R., Gonçalves D. R., Akras S., Gimeno G., Diaz R., Scharwächter J., Nuñez N. E., et al., 2019, *AJ*, 157, 156. doi:10.3847/1538-3881/ab0cf7
- Astropy Collaboration, Robitaille T. P., Tollerud E. J., Greenfield P., Droettboom M., Bray E., Aldcroft T., et al., 2013, *A&A*, 558, A33.
- Astropy Collaboration, Price-Whelan A. M., Sipőcz B. M., Günther H. M., Lim P. L., Crawford S. M., Conseil S., et al., 2018, *AJ*, 156, 123.
- Bailer-Jones C. A. L., 2015, *PASP*, 127, 994. doi:10.1086/683116
- Barden S. C., et al., 2010, *SPIE*, 7735, 773509, *SPIE*.77351
- Belczyński K., Mikołajewska J., Munari U., Ivison R. J., Friedjung M., 2000, *A&AS*, 146, 407
- Bennett P. D., Brown A., Fawcett S. M., Yang S., Bauer W. H., 2004, *ASPC*, 318, 222
- Blackburn J. K., 1995, *ASPC*, 77, 367, *ASPC*...77
- Bozzo E., Bahramian A., Ferrigno C., Sanna A., Strader J., Lewis F., Russell D. M., et al., 2018, *A&A*, 613, A22. doi:10.1051/0004-6361/201832588
- Bragaglia A., Duerbeck H. W., Munari U., Zwitter T., 1995, *A&A*, 297, 759
- Breeveld A. A., Landsman W., Holland S. T., Roming P., Kuin N. P. M., Page M. J., 2011, *AIPC*, 1358, 373, *AIPC*.1358
- Bressan A., Marigo P., Girardi L., Salasnich B., Dal Cero C., Rubele S., Nanni A., 2012, *MNRAS*, 427, 127. doi:10.1111/j.1365-2966.2012.21948
- Buder S., Sharma S., Kos J., Amarsi A. M., Nordlander T., Lind K., Martell S. L., et al., 2020, *arXiv*, arXiv:2011.02505
- Burrows D. N., et al., 2005, *SSRv*, 120, 165
- Cameron A. G. W., Fowler W. A., 1971, *ApJ*, 164, 111 doi:10.1086/150821
- Chen P. S., Liu J. Y., Shan H. G., 2019, *Ap&SS*, 364, 132. doi:10.1007/s10509-019-3620-2
- Cheung C. C., Donato D., Wallace E., Corbet R., Dubus G., Sokolovsky K., Takahashi H., 2010, *ATel*, 2487, 1
- Corradi R. L. M., Rodríguez-Flores E. R., Mampaso A., Greimel R., Viironen K., Drew J. E., Lennon D. J., et al., 2008, *A&A*, 480, 409. doi:10.1051/0004-6361:20078989
- Corradi R. L. M., Valentini M., Munari U., Drew J. E., Rodríguez-Flores E. R., Viironen K., Greimel R., et al., 2010, *A&A*, 509, A41. doi:10.1051/0004-6361/200913231
- Corradi R. L. M., Sabin L., Munari U., Cetrulo G., Englaro A., Angeloni R., Greimel R., et al., 2011, *A&A*, 529, A56. doi:10.1051/0004-6361/201016406
- Cutri R. M., Skrutskie M. F., van Dyk S., Beichman C. A., Carpenter J. M., Chester T., Cambresy L., et al., 2003, *yCat*, II/246
- de Laverny P., Recio-Blanco A., Worley C. C., Plez B., 2012, *A&A*, 544, A1261
- De Silva G. M., et al., 2015, *MNRAS*, 449, 2604
- Dimitrov V. V., Boeva S., Martí J., Bujalance-Fernández I., Sánchez-Ayaso E., Latev G. Y., Nikolov Y. M., et al., 2018, *arXiv*, arXiv:1811.03317
- Dobrzycka D., Kenyon S. J., Milone A. A. E., 1996, *AJ*, 111, 414
- Drew J. E., Greimel R., Irwin M. J., Aungwerojwit A., Barlow M. J., Corradi R. L. M., Drake J. J., et al., 2005, *MNRAS*, 362, 753. doi:10.1111/j.1365-2966.2005.09330.x
- Drilling J. S., Landolt A. U., 2000, in *Astrophysical Quantities*, 3rd ed., A.N. Cox ed., Springer-Verlag, 381
- Drozd K., Mikołajewska J., Darnley M., Hkiewicz K., Caldwell N., Shara M., 2019, *IAUS*, 339, 291. doi:10.1017/S174392131800279X
- Evans D. W., Riello M., De Angeli F., Carrasco J. M., Montegriffo P., Fabricius C., Jordi C., et al., 2018, *A&A*, 616, A4. doi:10.1051/0004-6361/201832756
- Evans P. A., Page K. L., Osborne J. P., Beardmore A. P., Willingale R., Burrows D. N., Kennea J. A., et al., 2019, *yCat*, IX/58
- Fluks M. A., Plez B., The P. S., de Winter D., Westerlund B. E., Steenman H. C., 1994, *A&AS*, 105, 311
- Forestini M., Charbonnel C., 1997, *A&AS*, 123, 241 doi:10.1051/aas:1997348
- Freeman K., Bland-Hawthorn J., 2002, *ARA&A*, 40, 4871
- Fujimoto M. Y., 1982, *ApJ*, 257, 767
- Gaia Collaboration, et al., 2018, *A&A*, 616, A11
- Gaia Collaboration, 2020, *yCat*, I/350
- Gehrels N., et al., 2004, *ApJ*, 611, 1005
- Giannini T., Nisini B., Antonucci S., Biazzo K., Alcalá J., Bacciotti F., Fedele D., et al., 2019, *A&A*, 631, A44. doi:10.1051/0004-6361/201936085
- Ginestet N., Carquillat J. M., 2002, *ApJS*, 143, 513. doi:10.1086/342942
- Giroletti M., Munari U., KÖrding E., Mioduszewski A., Sokoloski J., Cheung C. C., Corbel S., et al., 2020, *A&A*, 638, A130. doi:10.1051/0004-6361/202038142
- Gonçalves D. R., Magrini L., Munari U., Corradi R. L. M., Costa R. D. D., 2008, *MNRAS*, 391, L84. doi:10.1111/j.1745-3933.2008.00561.x
- Gonçalves D. R., Magrini L., Martins L. P., Teodorescu A. M., Quireza C., 2012, *MNRAS*, 419, 854. doi:10.1111/j.1365-2966.2011.19749.x

- Gonçalves D. R., Magrini L., de la Rosa I. G., Akras S., 2015, *MNRAS*, 447, 993. doi:10.1093/mnras/stu2437
- Gorlova N., Van Winckel H., Jorissen A., 2012, *BaltA*, 21, 165. doi:10.1515/astro-2017-0371
- Green G. M., Schlafly E., Zucker C., Speagle J. S., Finkbeiner D., 2019, *ApJ*, 887, 93. doi:10.3847/1538-4357/ab5362
- Grindlay J., Tang S., Simcoe R., Laycock S., Los E., Mink D., Doane A., et al., 2009, *ASPC*, 410, 101
- Gromadzki M., Mikołajewski M., Tomov T., Bellas-Velidis I., Dapergolas A., Galan C., 2006, *AcA*, 56, 97
- Gromadzki M., Mikołajewska J., Borawska M., Lednicka A., 2007, *BaltA*, 16, 37
- Gromadzki M., Mikołajewska J., Whitelock P., Marang F., 2009, *AcA*, 59, 169
- Gromadzki M., Mikołajewska J., Soszyński I., 2013, *AcA*, 63, 405
- Hartmann L., Herczeg G., Calvet N., 2016, *ARA&A*, 54, 135. doi:10.1146/annurev-astro-081915-023347
- Hellier C., 2001, *Cataclysmic Variable Stars*, Springer
- Henden A. A., Templeton M., Terrell D., Smith T. C., Levine S., Welch D., 2016, *yCat*, II/336
- Henize K. G., 1976, *ApJS*, 30, 491. doi:10.1086/190369
- Herwig F., 2005, *ARA&A*, 43, 435. doi:10.1146/annurev.astro.43.072103.150600
- Hill J. E., et al., 2004, *SPIE*, 5165, 217, *SPIE*.5165
- Hinkle K. H., Fekel F. C., Joyce R. R., Wood P., 2013, *ApJ*, 770, 28
- Hoffmeister C., Richter G., Wenzel W., 1985, *Variable Stars*, Springer-Verlag, Berlin
- Howell S. B., et al., 2014, *PASP*, 126, 3981
- Izzo L., Della Valle M., Mason E., Matteucci F., Romano D., Pasquini L., Vanzì L., et al., 2015, *ApJL*, 808, L14. doi:10.1088/2041-8205/808/1/L14
- Jorissen A., 2003, *ASPC*, 303, 25
- Jorissen A., Van Eck S., Dermine T., Van Winckel H., Gorlova N., 2012, *BaltA*, 21, 39. doi:10.1515/astro-2017-0356
- José J., Hernanz M., 1998, *ApJ*, 494, 680. doi:10.1086/305244
- Joy A. H., 1926, *ApJ*, 63, 281. doi:10.1086/142979
- Karaali S., Bilir S., Gökçe E. Y., 2013, *PASA*, 30, e011. doi:10.1017/pasa.2012.011
- Karovska M., 2006, *ESASP*, 604, 183, *ESASP*.604
- Kataoka J., Madejski G., Sikora M., Roming P., Chester M. M., Grupe D., Tsubuku Y., et al., 2008, *ApJ*, 672, 787. doi:10.1086/523093
- Kenyon S. J., 1986, *The Symbiotic Stars*, Cambridge Univ. Press
- Kenyon S. J., Livio M., Mikołajewska J., Tout C. A., 1993, *ApJL*, 407, L81. doi:10.1086/186811
- Kenyon S. J., Fernandez-Castro T., 1987, *AJ*, 93, 938
- Kenyon S. J., Webbink R. F., 1984, *ApJ*, 279, 252. doi:10.1086/161888
- Kippenhahn R., 1955, *AN*, 282, 73. doi:10.1002/asna.19552820204
- Kniazev A. Y., Väisänen P., Whitelock P. A., Menzies J. W., Feast M. W., Grebel E. K., Buckley D. A. H., et al., 2009, *MNRAS*, 395, 1121. doi:10.1111/j.1365-2966.2009.14617.x
- Kochanek C. S., et al., 2017, *PASP*, 129, 104502
- Kolotilov E. A., Munari U., Popova A. A., Tatarnikov A. M., Shenavrin V. I., Yudin B. F., 1998, *AstL*, 24, 451
- Koornneef J., 1983, *A&A*, 500, 247
- Kos J., et al., 2017, *MNRAS*, 464, 12591
- Kumar V., Srivastava M. K., Banerjee D. P. K., Joshi V., 2021, *MNRAS*, 500, L12. doi:10.1093/mnras/laaa159
- Kuranov, A.G., & Postnov, K.A. 2015, *Astron. Lett.*, 41, 114
- Landolt A. U., 1992, *AJ*, 104, 340. doi:10.1086/116242
- Lindgren L., Bastian U., Biermann M., Bombrun A., de Torres A., Gerlach E., Geyer R., et al., 2020, *arXiv*, arXiv:2012.01742
- Lee T. A., 1970, *ApJ*, 162, 217
- Lopes de Oliveira, R., Sokoloski, J.L., Luna, G.J.M., Mukai, K., & Nelson, T. 2018, *ApJ*, 864, 46
- Lü G., Yungelson L., Han Z., 2006, *MNRAS*, 372, 1389. doi:10.1111/j.1365-2966.2006.10947.x
- Lü G.-L., Zhu C.-H., Postnov K. A., Yungelson L. R., Kuranov A. G., Wang N., 2012, *MNRAS*, 424, 2265. doi:10.1111/j.1365-2966.2012.21395.x
- Lucy A. B., Sokoloski J. L., Munari U., Roy N., Kuin N. P. M., Rupen M. P., Knigge C., et al., 2020, *MNRAS*, 492, 3107. doi:10.1093/mnras/stz3595
- Luna G. J. M., Sokoloski J. L., Mukai K., Nelson T., 2013, *A&A*, 559, A6. doi:10.1051/0004-6361/201220792
- Luri X., Brown A. G. A., Sarro L. M., Arenou F., Bailer-Jones C. A. L., Castro-Ginard A., de Bruijne J., et al., 2018, *A&A*, 616, A9. doi:10.1051/0004-6361/201832964
- Lutovinov A., Suleimanov V., Manuel Luna G. J., Sazonov S., de Martino D., Ducci L., Doroshenko V., et al., 2020, *NewAR*, 91, 101547. doi:10.1016/j.newar.2020.101547
- Marigo P., Girardi L., Bressan A., Rosenfield P., Aringer B., Chen Y., Dussini M., et al., 2017, *ApJ*, 835, 77. doi:10.3847/1538-4357/835/1/77
- Martell S. L., et al., 2017, *MNRAS*, 465, 32031
- Masetti N., Orlandini M., Palazzi E., Amati L., Frontera F., 2006, *A&A*, 453, 295. doi:10.1051/0004-6361:20065025
- Masetti N., Rigon E., Maiorano E., Cusumano G., Palazzi E., Orlandini M., Amati L., et al., 2007a, *A&A*, 464, 277. doi:10.1051/0004-6361:20066517
- Masetti N., Landi, R., Pretorius, M. L., et al. 2007b, *A&A*, 470, 331
- Masetti N., Munari U., Henden A. A., Page K. L., Osborne J. P., Starrfield S., 2011, *A&A*, 534, A89. doi:10.1051/0004-6361/201117260
- Massey P., 2002, *ApJS*, 141, 81. doi:10.1086/338286
- Mendigutía I., Calvet N., Montesinos B., Mora A., Muzerolle J., Eiroa C., Oudmajer R. D., et al., 2011, *A&A*, 535, A99. doi:10.1051/0004-6361/201117444
- Merc J., Gális R., Wolf M., 2019a, *AN*, 340, 598. doi:10.1002/asna.201913662
- Merc J., Gális R., Wolf M., 2019b, *RNAAS*, 3, 28. doi:10.3847/2515-5172/ab0429
- Merloni A., Predehl P., Becker W., Böhringer H., Boller T., Brunner H., Brusa M., et al., 2012, *arXiv*, arXiv:1209.3114
- Merrill P. W., 1940, *The Spectra of Long-Period Variable Stars*, Univ. Chicago Press
- Merrill P. W., Burwell C. G., 1950, *ApJ*, 112, 72. doi:10.1086/145319
- Mikołajewska J., 2003, *ASPC*, 303, 9
- Mikołajewska J., Caldwell N., Shara M. M., 2014, *MNRAS*, 444, 586. doi:10.1093/mnras/stu1480
- Mikołajewska J., Shara M. M., Caldwell N., Iłkiewicz K., Zurek D., 2017, *MNRAS*, 465, 1699. doi:10.1093/mnras/stw2937
- Mikołajewski M., Mikołajewska J., Tomov T., Kulesza B., Szczerba R., Wikierski B., 1990, *AcA*, 40, 129
- Miszalski B., Mikołajewska J., 2014, *MNRAS*, 440, 1410. doi:10.1093/mnras/stu292
- Miszalski B., Mikołajewska J., Udalski A., 2013, *MNRAS*, 432, 3186. doi:10.1093/mnras/stt673
- Mohamed S., Podsiadlowski P., 2012, *BaltA*, 21, 88. doi:10.1515/astro-2017-0362
- Molaro P., Izzo L., Mason E., Bonifacio P., Della Valle M., 2016, *MNRAS*, 463, L117. doi:10.1093/mnras/slt169
- Molaro P., Izzo L., Bonifacio P., Hernanz M., Selvelli P., della Valle M., 2020, *MNRAS*, 492, 4975. doi:10.1093/mnras/stz3587
- Morgan D. H., 1992, *MNRAS*, 258, 639. doi:10.1093/mnras/258.3.639
- Morgan W. W., Keenan P. C., 1973, *ARA&A*, 11, 29
- Morgan W. W., Keenan P. C., Kellman E., 1943, *An Atlas of Stellar Spectra*, Chicago Univ. Press
- Mukai K., et al., 2016, *MNRAS*, 461, L1 (Mk16)
- Munari, U., in *The Impact of Binary Stars on Stellar Evolution*, G. Beccari and H.M.J. Boffin eds., 2019, Cambridge Univ. Press.p. 77 (arXiv:190901389)
- Munari U., Margoni R., Stagni R., 1990, *MNRAS*, 242, 653
- Munari U., Renzini A., 1992, *ApJL*, 397, L87
- Munari U., Jurdana-Šepić R., 2002, *A&A*, 386, 237. doi:10.1051/0004-6361:20020201
- Munari U., Moretti S., 2012, *BaltA*, 21, 22. doi:10.1515/astro-2017-0354
- Munari U., Dallaporta S., Cherini G., 2016, *NewA*, 47, 7
- Munari U., Joshi V., Banerjee D. P. K., Čotar K., Shugarov S. Y., Jurdana-Šepić R., et al., 2019, *MNRAS*, 488, 5536. doi:10.1093/mnras/stz2078
- Munari U., Valisa P., Vagnozzi A., Dallaporta S., Hamsbich F. J., Frigo A.,

- 2021, *CoSka* 51, 103
- Núñez N. E., Nelson T., Mukai K., Sokoloski J. L., Luna G. J. M., 2016, *ApJ*, 824, 23. doi:10.3847/0004-637X/824/1/23
- O'Brien T. J., Bode M. F., Porcas R. W., Muxlow T. W. B., Eyres S. P. S., Beswick R. J., Garrington S. T., et al., 2006, *Natur*, 442, 279. doi:10.1038/nature04949
- Pantaleoni González M., Maíz Apellániz J., Barbá R. H., Negueruela I., 2020, *RNAAS*, 4, 12. doi:10.3847/2515-5172/ab712b
- Pastorelli G., Marigo P., Girardi L., Aringer B., Chen Y., Rubele S., Trabucchi M., et al., 2020, *MNRAS*, 498, 3283. doi:10.1093/mnras/staa2565
- Pearse R. W. B., Gaydon A. G., 1976, *The Identification of Molecular Spectra*, 4th ed., Chapman and Hall, London
- Poole T. S., et al., 2008, *MNRAS*, 383, 627
- Pugh T., Gray D. F., Griffin R. F., 2015, *MNRAS*, 454, 2344. doi:10.1093/mnras/stv2003
- Ricker G. R., et al., 2015, *JATIS*, 1, 0140031
- Rodríguez-Flores E. R., Corradi R. L. M., Mampaso A., García-Alvarez D., Munari U., Greimel R., Rubio-Díez M. M., et al., 2014, *A&A*, 567, A49. doi:10.1051/0004-6361/201323182
- Roming P. W. A., et al., 2005, *SSRv*, 120, 95
- Roth M. M., Sandin C., Kamann S., Husser T.-O., Weilbacher P. M., Monreal-Ibero A., Bacon R., et al., 2018, *A&A*, 618, A3. doi:10.1051/0004-6361/201833007
- Rukeya R., Lü G., Wang Z., Zhu C., 2017, *PASP*, 129, 074201. doi:10.1088/1538-3873/aa6b4d
- Sabbadin F., Falomo R., Ortolani S., 1987, *A&AS*, 67, 541
- Sahai R., Sanz-Forcada J., Sánchez Contreras C., Stute M., 2015, *ApJ*, 810, 77. doi:10.1088/0004-637X/810/1/77
- Sanduleak N., Stephenson C. B., 1973, *ApJ*, 185, 899. doi:10.1086/152464
- Schlafly E. F., Finkbeiner D. P., 2011, *ApJ*, 737, 103
- Sekeráš M., Skopal A., Shugarov S., Shagatova N., Kundra E., Komžík R., Vrašák M., et al., 2019, *CoSka*, 49, 19
- Shappee B. J., et al., 2014, *ApJ*, 788, 48
- Sharma S., et al., 2018, *MNRAS*, 473, 20041
- Sheinis A., et al., 2015, *JATIS*, 1, 0350021
- Siess L., Livio M., Lattanzio J., 2002, *ApJ*, 570, 329. doi:10.1086/339733
- Skopal A., 2005, *A&A*, 440, 995. doi:10.1051/0004-6361:20034262
- Skopal A., Cariková Z., 2015, *A&A*, 573, A8. doi:10.1051/0004-6361/201424779
- Skopal A., Vittone A. A., Errico L., Otsuka M., Tamura S., Wolf M., Elkin V. G., 2006, *A&A*, 453, 279. doi:10.1051/0004-6361:20052917
- Skopal A., Vaňko M., Pribulla T., Chochol D., Semkov E., Wolf M., Jones A., 2007, *AN*, 328, 909. doi:10.1002/asna.200710822
- Skopal A., Shugarov S., Vaňko M., Dubovský P., Peneva S. P., Semkov E., Wolf M., 2012, *AN*, 333, 242. doi:10.1002/asna.201111655
- Skrutskie M. F., et al., 2006, *AJ*, 131, 11631
- Slovak M. H., Africano J., 1978, *MNRAS*, 185, 591
- Sokoloski J. L., Bildsten L., 1999, *ApJ*, 517, 919. doi:10.1086/307234
- Sokoloski J. L., Bildsten L., Ho W. C. G., 2001, *MNRAS*, 326, 553
- Sokoloski J. L., Kenyon S. J., Espey B. R., Keyes C. D., McCandliss S. R., Kong A. K. H., Aufdenberg J. P., et al., 2006, *ApJ*, 636, 1002. doi:10.1086/498206
- Sokoloski J. L., Lawrence S., Crotts A. P. S., Mukai K., 2017, *arXiv*, arXiv:1702.05898
- Sowell J. R., Trippie M., Caballero-Nieves S. M., Houk N., 2007, *AJ*, 134, 1089. doi:10.1086/520060
- Starrfield, S., Iliadis, C., Hix, W. R. 2008, in *Classical Novae* 2nd ed., M. F. Bode and A. Evans eds., CAS 43, Cambridge Univ. Press.
- Starrfield S., Bose M., Iliadis C., Hix W. R., Woodward C. E., Wagner R. M., 2020, *ApJ*, 895, 70. doi:10.3847/1538-4357/ab8d23
- Sterken C., Jäschek C., 2005, eds. *Light Curves of Variable Stars*, Cambridge Univ. Press
- Stoyanov K. A., Martí J., Zamanov R., Dimitrov V. V., Kurtenkov A., Sánchez-Ayaso E., Bujalance-Fernández I., et al., 2018, *BlaAJ*, 28, 42
- Tajitsu A., Sadakane K., Naito H., Arai A., Aoki W., 2015, *Natur*, 518, 381. doi:10.1038/nature14161
- Tatarnikova A. A., Marrese P. M., Munari U., Tomov T., Whitelock P. A., Yudin B. F., 2003, *MNRAS*, 344, 1233. doi:10.1046/j.1365-8711.2003.06911.x
- Tomov T., Kolev D., Ivanov M., Antov A., Jones A., Mikolajewski M., Lepardo A., et al., 1996, *A&AS*, 116, 1
- Turnshek D. E., Turnshek D. A., Craine E. R., Boeshaar, P. C., 1985, *An Atlas of Digital Spectra of Cool Stars*, Western Research Co., Tucson
- Walker A. R., 1983, *MNRAS*, 203, 25. doi:10.1093/mnras/203.1.25
- Wallerstein G., Harrison T., Munari U., Vanture A., 2008, *PASP*, 120, 492. doi:10.1086/587965
- Warner B., 1995, *Cataclysmic Variable Stars*, CAS 28, Cambridge Univ. Press
- Wittenmyer R. A., et al., 2018, *AJ*, 155, 841
- Woodward C. E., Pavlenko Y. V., Evans A., Wagner R. M., Ilyin I., Strassmeier K. G., Starrfield S., et al., 2020, *AJ*, 159, 231. doi:10.3847/1538-3881/ab8639
- Yamashita Y., Nariai K., 1977, *An Atlas of Representative Stellar Spectra*, Univ. of Tokyo Press
- Yang H., Herczeg G. J., Linsky J. L., Brown A., Johns-Krull C. M., Ingleby L., Calvet N., et al., 2012, *ApJ*, 744, 121. doi:10.1088/0004-637X/744/2/121
- Yungelson L., Livio M., Tutukov A., Kenyon S. J., 1995, *ApJ*, 447, 656. doi:10.1086/175908
- Yungelson L. R., Kuranov A. G., Postnov K. A., 2019, *MNRAS*, 485, 851. doi:10.1093/mnras/stz467
- Zamanov R., Boeva S., Stoyanov K., Bode M. F., Antov A., Bachev R., 2011, *IBVS*, 5995, 1
- Zamanov R. K., Boeva S., Nikolov Y. M., Petrov B., Bachev R., Latev G. Y., Popov V. A., et al., 2017, *AN*, 338, 680. doi:10.1002/asna.201713362
- Zamanov R., Stoyanov K., Nikolov G., Kurtenkov A., Boeva S., Latev G., Tomov T., 2019, *ATel*, 13236
- Zamanov R. K., Boeva S., Stoyanov K. A., Latev G., Spassov B., Kurtenkov A., Nikolov G., 2020, *AN*, 341, 430. doi:10.1002/asna.202013730
- Zhekov S. A., Tomov T. V., 2019, *MNRAS*, 489, 2930. doi:10.1093/mnras/stz2329
- Zhu C., Lü G., Wang Z., Zhang J., 2010, *NewA*, 15, 144. doi:10.1016/j.newast.2009.07.002

APPENDIX A: ADDITIONAL TABLES AND FIGURES

In this section, we present ancillary information that might be useful to the interested reader. First, we provide some details that concern follow-up observations of 33 candidate *acc*-SySt when searching for signs of the near-UV upturn (Table A1) and flickering (Table A4). Furthermore, we compute values for the position and luminosity for the 33 systems based on information given by the cross-match with external catalogues in Table A2. The radial velocity information measured or collected for some of the 33 program stars in Table 6 is expanded for comparison reasons to include some GALAH radially pulsating and field M giants in Table A3. The list of VVCep stars discussed in sect. 4.8 is provided in Table A5. Finally, Fig. A1 displays the region of high S/N normalised template spectra around H α and H β lines. These templates were used for subtraction from program star spectra in order to detect prominent H α emission features, with details of the subtraction results complemented by the ASAS-SN *V*-filter lightcurves plotted in Fig. A2 to A8.

Table A1. Log of low-resolution spectroscopic observations obtained with the Asiago 1.22m + B&C + 300 ln/mm (3300-8000 Å, 2.31 Å/pix) in search for the near-UV upturn. The exposure time is in seconds.

SySt	UT middle	expt
GaSS 1-7	2020-06-18 20:40	120
GaSS 1-7	2020-06-27 20:32	960
GaSS 1-9	2019-08-09 19:59	480
GaSS 1-9	2019-08-16 19:43	480
GaSS 1-9	2019-09-01 19:48	1200
GaSS 1-9	2020-06-27 22:31	960
GaSS 1-9	2020-08-25 19:18	480
GaSS 1-12	2019-08-16 20:27	720
GaSS 1-12	2019-08-19 20:54	960
GaSS 1-12	2019-09-01 19:27	1200
GaSS 1-12	2020-08-25 20:11	480
GaSS 1-13	2020-08-25 21:37	480
GaSS 1-13	2020-10-13 18:05	1800
GaSS 1-14	2019-08-30 18:59	480
GaSS 1-14	2019-09-01 20:18	960
GaSS 1-14	2019-12-06 17:24	1200
GaSS 1-15	2020-09-02 21:58	960
GaSS 1-15	2020-10-13 19:49	1800
GaSS 1-21	2020-06-19 21:24	720
GaSS 1-21	2020-06-27 21:54	1200
GaSS 1-23	2019-08-16 19:57	1200
GaSS 1-23	2019-08-19 19:41	960
GaSS 1-23	2019-09-01 19:58	1200
GaSS 1-23	2020-08-25 19:37	480
GaSS 1-25	2020-08-25 19:27	480
GaSS 1-28	2019-09-03 19:44	1200
GaSS 1-31	2020-08-25 20:20	480
GaSS 1-31	2020-10-13 17:30	1800
GaSS 1-33	2020-08-27 22:18	1440
GaSS 1-33	2020-10-13 20:28	3600

Table A2. Gaia *eDR3* parallax and its uncertainty for the program stars, distance and height above the Galactic plane for stars with $\sigma(\pi)/\pi < 0.2$, and corresponding absolute *V* and *K_s* magnitudes from APASS and 2MASS values.

	<i>eDR3</i>		d (kpc)	z (kpc)	M(V) (mag)	M(K _s) (mag)
	π	err(π)				
GaSS 1-1	0.0149	0.0125				
GaSS 1-2	0.0249	0.0114				
GaSS 1-3	0.1216	0.0100	8.2	3.7	-2.2	-5.8
GaSS 1-4	0.1226	0.0169	8.2	3.6	-2.2	-6.1
GaSS 1-5	0.0988	0.0157	10.1	5.0	-1.7	-5.5
GaSS 1-6	0.1843	0.0218	5.4	1.8	-1.7	-5.9
GaSS 1-7	0.0476	0.0216				
GaSS 1-8	0.1358	0.0153	7.4	2.8	-2.1	-5.6
GaSS 1-9	0.0974	0.0311				
GaSS 1-10	0.0715	0.0159				
GaSS 1-11	0.1523	0.0263	6.6	1.2	-2.3	-6.9
GaSS 1-12	0.2183	0.0321	4.6	0.9	-1.9	-7.1
GaSS 1-13	0.0423	0.0223				
GaSS 1-14	0.1163	0.0170	8.6	3.4	-1.8	-6.0
GaSS 1-15	0.3503	0.0257	2.9	1.4	-0.5	-4.5
GaSS 1-16	0.0219	0.0137				
GaSS 1-17	0.1861	0.0111	5.4	1.9	-2.5	-6.2
GaSS 1-18	0.1154	0.0157	8.7	3.5	-1.8	-5.6
GaSS 1-19	0.0589	0.0125				
GaSS 1-20	0.1327	0.0343				
GaSS 1-21	0.0391	0.0247				
GaSS 1-22	0.1711	0.0218	5.8	1.8	-2.7	-6.6
GaSS 1-23	0.2094	0.0245	4.8	1.3	-1.5	-6.0
GaSS 1-24	0.0902	0.0233				
GaSS 1-25	0.2306	0.0183	4.3	0.8	-2.3	-6.1
GaSS 1-26	0.0633	0.0171				
GaSS 1-27	0.2143	0.0177	4.7	1.3	-2.3	-5.7
GaSS 1-28	0.1326	0.0187	7.5	1.8	-1.4	-5.8
GaSS 1-29	0.1422	0.0157	7.0	2.7	+0.1	-5.3
GaSS 1-30	0.1799	0.0194	5.6	1.8	-2.7	-6.5
GaSS 1-31	0.2344	0.0170	4.3	1.1	-2.3	-6.1
GaSS 1-32	0.1877	0.0228	5.3	1.7	-2.5	-6.4
GaSS 1-33	0.0665	0.0327				

Table A3. Heliocentric radial velocity of some GALAH radially pulsating and field M giants observed along with the candidate symbiotic stars of Table 6. The values measured with the Asiago 1.82m telescope + Echelle spectrograph are compared with the corresponding values of rv_guess listed in GALAH DR3. The mean radial velocity listed in Gaia DR2 is also given, with its formal uncertainty and the number of epoch transits over which it has been computed.

RA	DEC	Asiago 1.82m Echelle			GALAH DR3			Gaia DR2		
		UT middle	RV_{\odot} (km/s)	err (km/s)	UT middle	RV_{\odot} (km/s)	err (km/s)	$\langle RV_{\odot} \rangle$ (km/s)	err (km/s)	N
<i>radial pulsators</i>										
19 17 30.06	-18 47 02.1	2020-10-30 17:16	-28.14	0.51	2017-05-07 18:28	-34.63	0.03	-32.82	2.87	2
20 35 04.52	-05 47 35.3	2020-10-29 17:32	-120.82	1.13	2014-07-09 15:39	-121.61	0.21			
23 31 17.83	-00 30 39.4	2019-12-09 18:30	-34.67	0.49	2017-07-24 17:27	-37.11	0.37	-35.81	0.93	6
		2020-01-15 17:06	-36.17	0.33						
		2020-10-29 19:59	-39.47	0.31						
<i>other GALAH M giants</i>										
03 40 25.30	14 30 00.6	2020-01-13 20:42	11.46	0.21	2016-01-10 10:47	9.94	0.48	9.45	0.70	6
05 21 50.50	01 51 26.8	2019-12-07 01:50	-16.54	0.29	2015-08-30	-14.65		-16.44	1.84	6
		2020-01-13 20:56	-17.47	0.10	2015-12-27 13:09	-12.42	0.31			
06 19 12.30	-17 35 20.8	2020-01-13 22:17	121.14	0.43	2017-01-06 13:35	120.96	0.40	121.47	0.80	7
10 00 41.60	-21 35 54.7	2020-04-10 20:13	188.45	0.58	2016-04-24 09:55	189.81	0.61	191.32	1.02	6
10 32 55.50	12 51 30.4	2020-04-10 20:34	132.32	0.12	2017-02-05 15:42	131.48	0.39	135.27	1.79	3
10 51 30.19	00 43 59.5	2020-04-10 21:04	165.91	0.36	2017-01-27 14:10	163.82	0.33	163.32	0.82	2
12 08 10.13	-09 07 52.8	2020-04-10 21:50	45.34	0.22	2016-04-03 12:48	47.24	0.33	45.68	0.43	20
12 16 50.58	-06 31 19.3	2020-04-10 22:04	83.14	0.19	2017-01-31 15:22	81.32	0.63	83.23	0.32	28
17 19 00.39	-17 45 42.9	2020-07-05 21:21	-23.56	0.91	2017-05-09 15:29	-23.62	0.61			
19 59 58.75	08 04 07.3	2020-10-29 16:57	-57.45	0.05	2016-10-08 09:34	-57.27	0.02	-57.85	0.15	3
20 00 03.82	07 22 39.7	2020-10-31 16:52	3.28	0.02	2016-10-08 09:34	2.65	0.15	2.14	0.14	14
20 05 15.00	08 54 02.5	2020-10-31 16:59	-0.49	0.05	2016-05-31 19:34	-0.07	0.24	-1.14	0.42	6
22 04 33.89	-08 14 49.9	2020-10-29 20:43	20.63	0.18	2014-07-11 17:59	19.40	0.01			
22 34 17.16	-05 04 57.7	2020-10-29 20:55	-20.77	0.52	2015-11-11 10:06	-19.89	0.09			

Table A4. *B* and *V* photometry of the candidate *acc*-SySt as measured during the search for flickering. The given HJD is the middle UT of the 70min duration of the time-series photometry.

	HJD (-2459000)	<i>B</i> (mag)	<i>V</i> (mag)
GaSS 1-1	117.834	14.248	13.078
GaSS 1-2	117.878	14.374	12.899
GaSS 1-3	102.882	14.067	12.497
GaSS 1-9	94.496	15.429	13.321
GaSS 1-11	95.543	13.825	12.083
GaSS 1-12	96.546	13.874	12.122
GaSS 1-13	97.497	15.605	13.641
GaSS 1-14	129.530	14.792	12.976
GaSS 1-15	97.549	13.838	12.092
GaSS 1-16	124.865	15.125	13.385
GaSS 1-17	120.852	13.137	11.419
GaSS 1-21	130.986	15.921	14.010
GaSS 1-23	94.546	15.419	13.301
GaSS 1-25	122.525	13.441	11.541
GaSS 1-26	146.505	15.427	13.723
GaSS 1-27	96.496	12.746	11.213
GaSS 1-28	128.526	15.415	13.566
GaSS 1-30	124.526	12.964	11.213
GaSS 1-31	125.504	13.007	11.193
GaSS 1-32	126.502	13.336	11.473
GaSS 1-33	130.531	17.076	15.403

Table A5. The VVCep stars selected from the catalog of [Pantaleoni González et al. \(2020\)](#). The distance, height over the galactic plane and absolute infrared magnitude $M(K_S)$ are computed from Gaia $eDR3$ and 2MASS values.

name	RA	DEC	dist (kpc)	z (pc)	K_S (mag)	$M(K_S)$ (mag)	spectrum	
V641 Cas	00 09 26.3	+63 57 14	2.9	75	1.7	-10.8	M3	Iab
KN Cas	00 09 36.4	+62 40 04	4.6	15	4.3	-9.3	M1	Iab
V554 Cas	01 10 20.1	+62 30 40	2.6	-13	2.7	-9.8	M2	I
AZ Cas	01 42 16.5	+61 25 16	3.3	-49	4.1	-8.9	M0	Ib
XX Per	02 03 09.4	+55 13 57	2.5	-274	2.0	-10.1	M4	Ib
HDE 237006	02 49 08.8	+58 00 48	2.5	-59	3.1	-9.2	M1	Ib
WY Gem	06 11 56.2	+23 12 25	1.9	76	1.9	-9.7	M2	Iab
V926 Mon	07 02 06.7	-03 45 17	1.1	12	2.0	-8.2	M2	Ib
KQ Pup	07 33 48.0	-14 31 26	0.7	33	0.1	-9.3	M2	Iab
V624 Pup	08 00 41.4	-32 50 25	5.0	-125	4.2	-9.5	M2	Iab
WY Vel	09 21 59.1	-52 33 52	1.9	-61	0.4	-11.3	M3	Ib:
HDE 300933	10 38 03.0	-56 49 02	3.1	79	1.8	-10.8	M2	Iab/Ib
V730 Car	10 44 57.3	-59 56 06	2.4	-36	2.5	-9.6	M1	Iab
HD 101007	11 36 56.9	-61 10 58	2.1	15	2.0	-9.8	M3	Ib
V772 Cen	11 41 49.4	-63 24 52	2.3	-65	2.1	-9.9	M2	Ib
CD-61.3575	12 44 16.1	-61 56 21	2.2	35	1.6	-10.3	M2	Ia
CD-58.6089	15 34 41.4	-58 42 40	4.1	-163	3.4	-9.8	M2	Ib
α Sco	16 29 24.5	-26 25 55	0.2	46	-4.1	-10.3	M0.5	Iab
FR Sct	18 23 22.8	-12 40 52	2.4	14	2.1	-10.4	M2.5	Iab
V381 Cep	21 19 15.7	+58 37 25	1.8	201	0.8	-10.8	M1	Ib
VV Cep	21 56 39.1	+63 37 32	1.0	123	-0.0	-10.2	M2	Ia-Iab
HDE 235749	22 11 35.7	+55 16 04	4.0	-55	3.3	-9.9	M2	Ib
U Lac	22 47 43.4	+55 09 30	4.2	-263	1.9	-11.4	M4	Iab

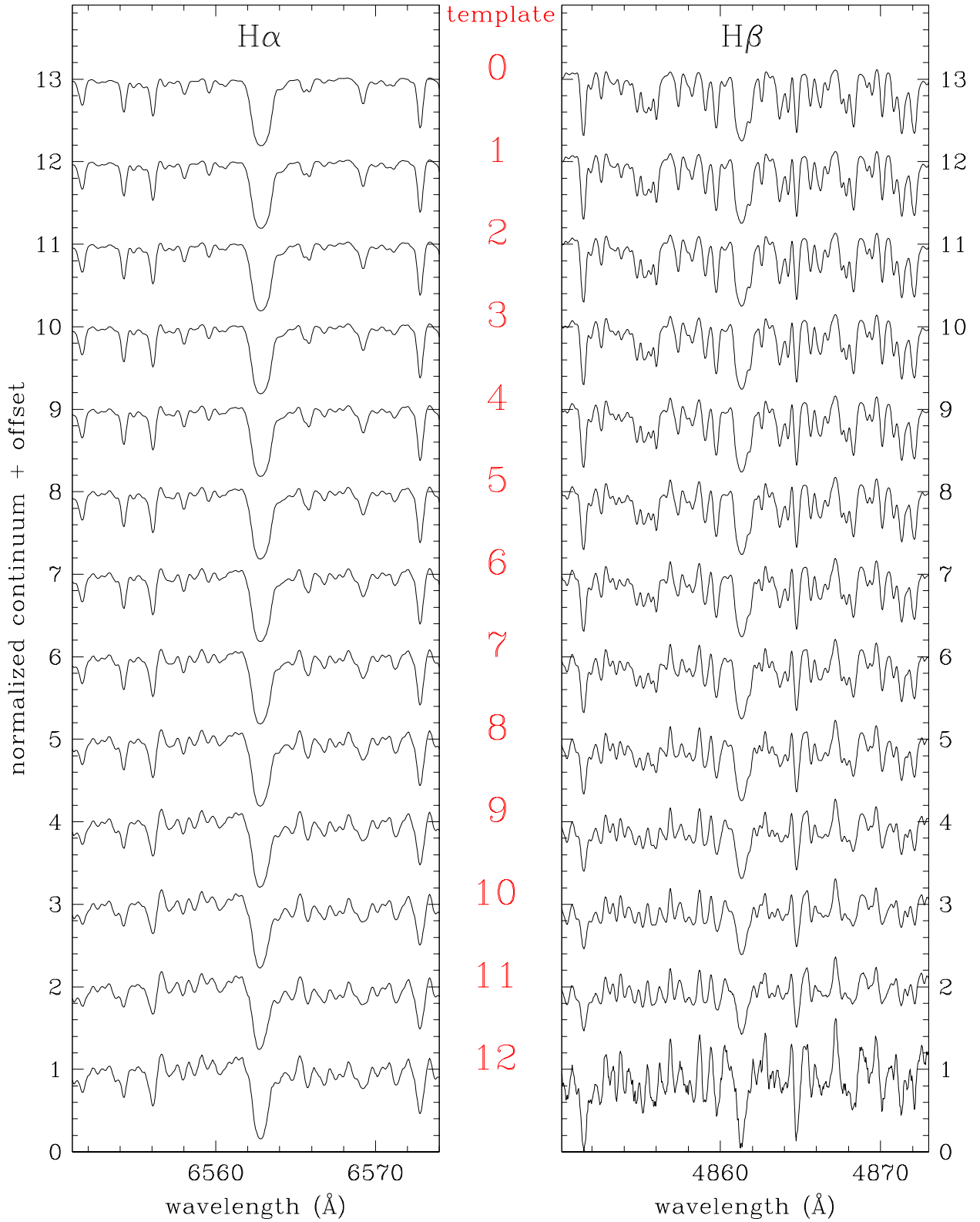


Figure A1. Sequence of templates as listed in Table 4. The template label/bin is indicated in red, and the template spectra are ordered from earlier to later M-type going from top to bottom. The bottom-most spectrum is of relatively lower S/N due to the small number of spectra that were used in constructing this template (see Table 4).

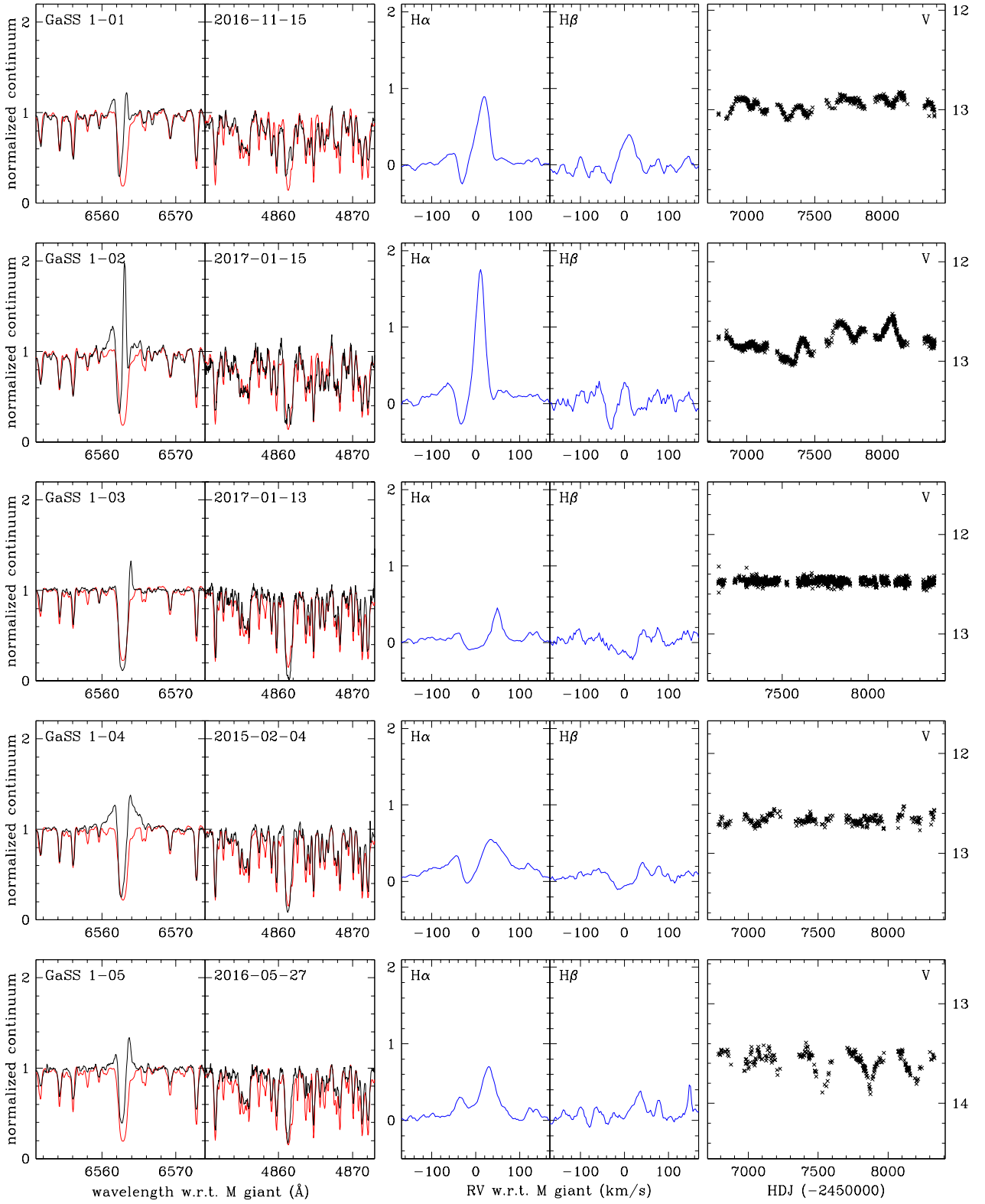


Figure A2. Left-most panels: H α and H β profiles (in black) compared to respective templates (in red) for program stars GaSS 1-1 to GaSS 1-5. Center panels: the result of subtracting the template from the object spectrum. Right-most panel: V-filter lightcurve from ASAS-SN sky patrol data.

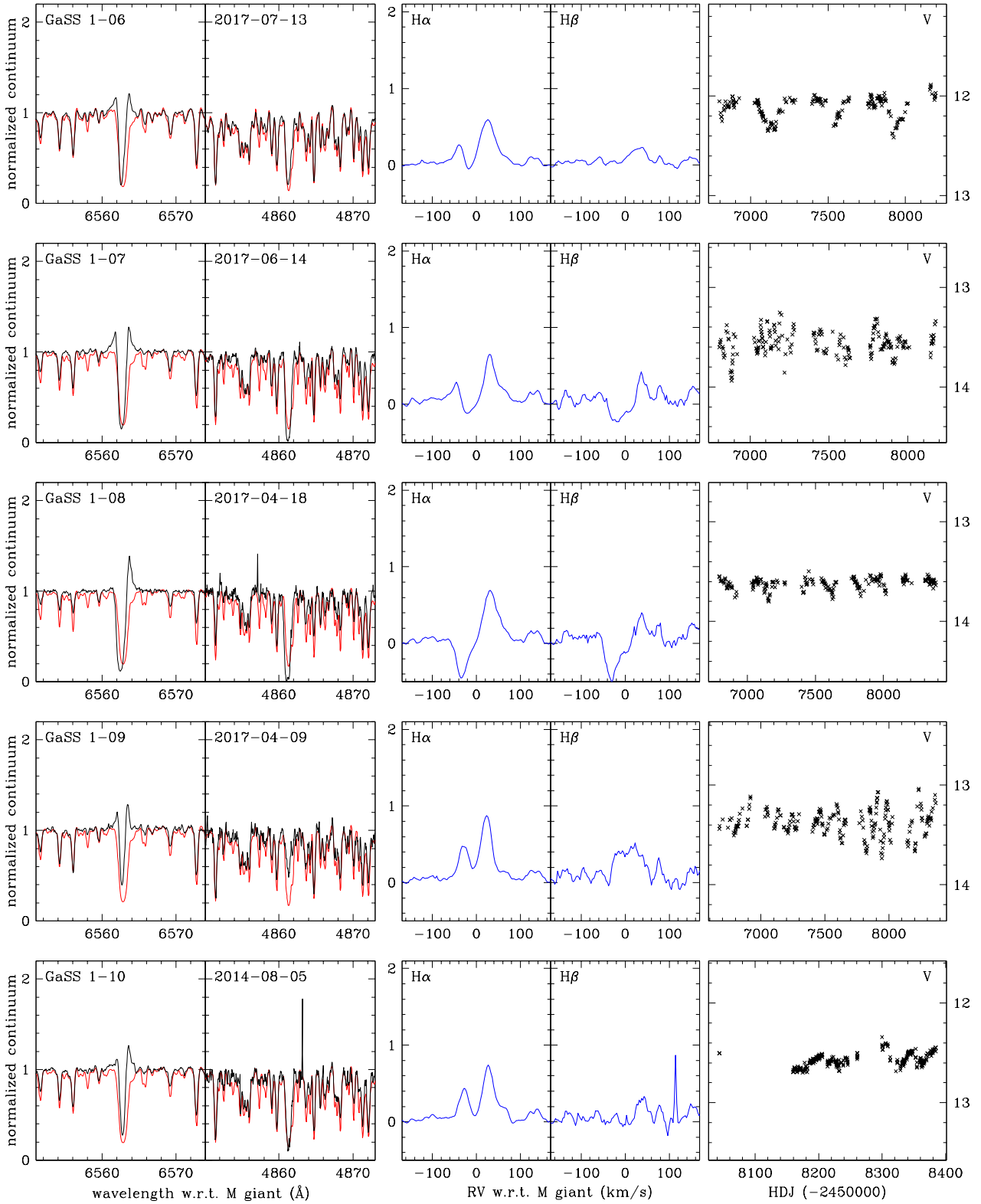


Figure A3. Similar to Fig. A2 for program stars GaSS 1-6 to GaSS 1-10.

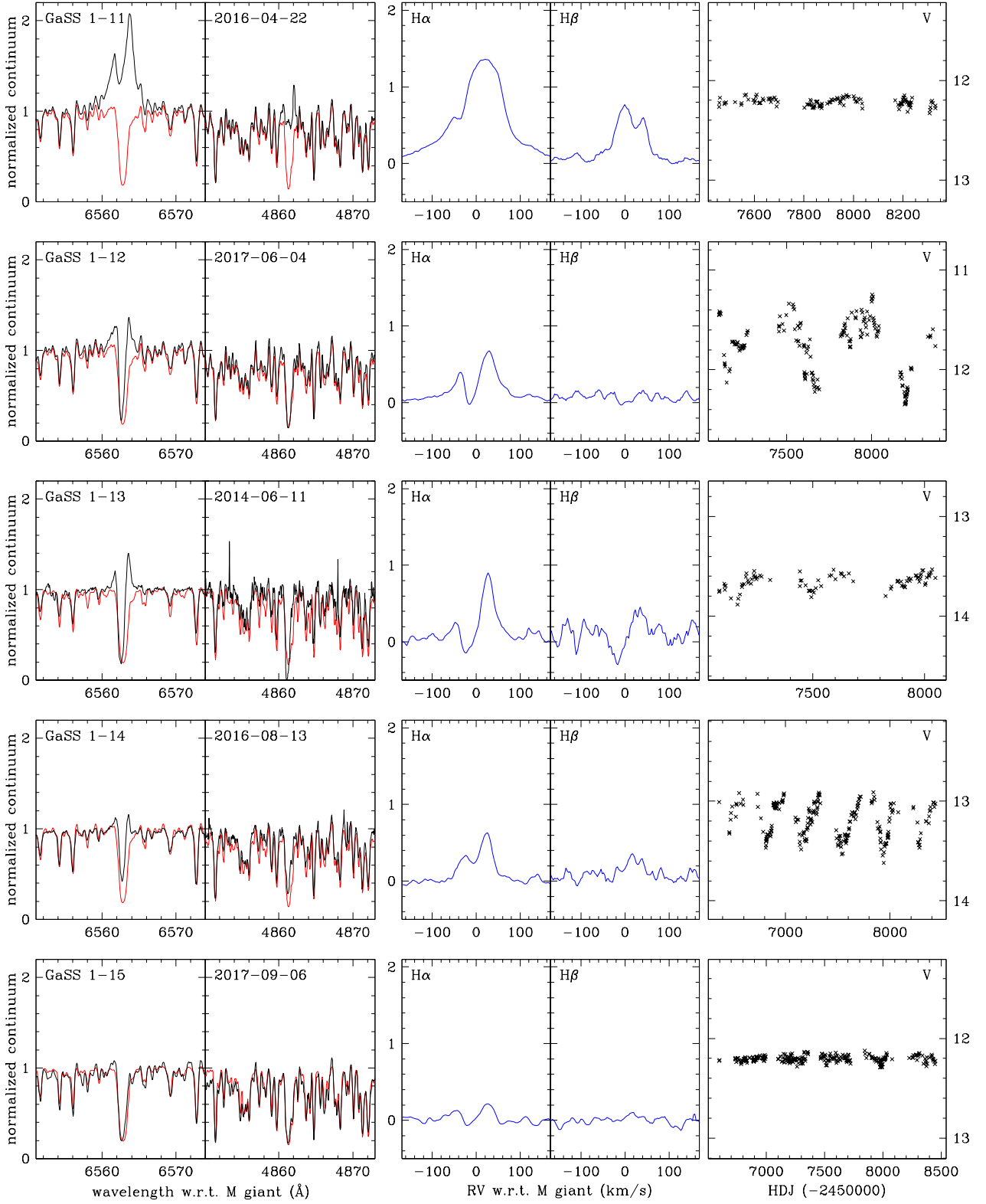


Figure A4. Similar to Fig. A2 for program stars GaSS 1-11 to GaSS 1-16.

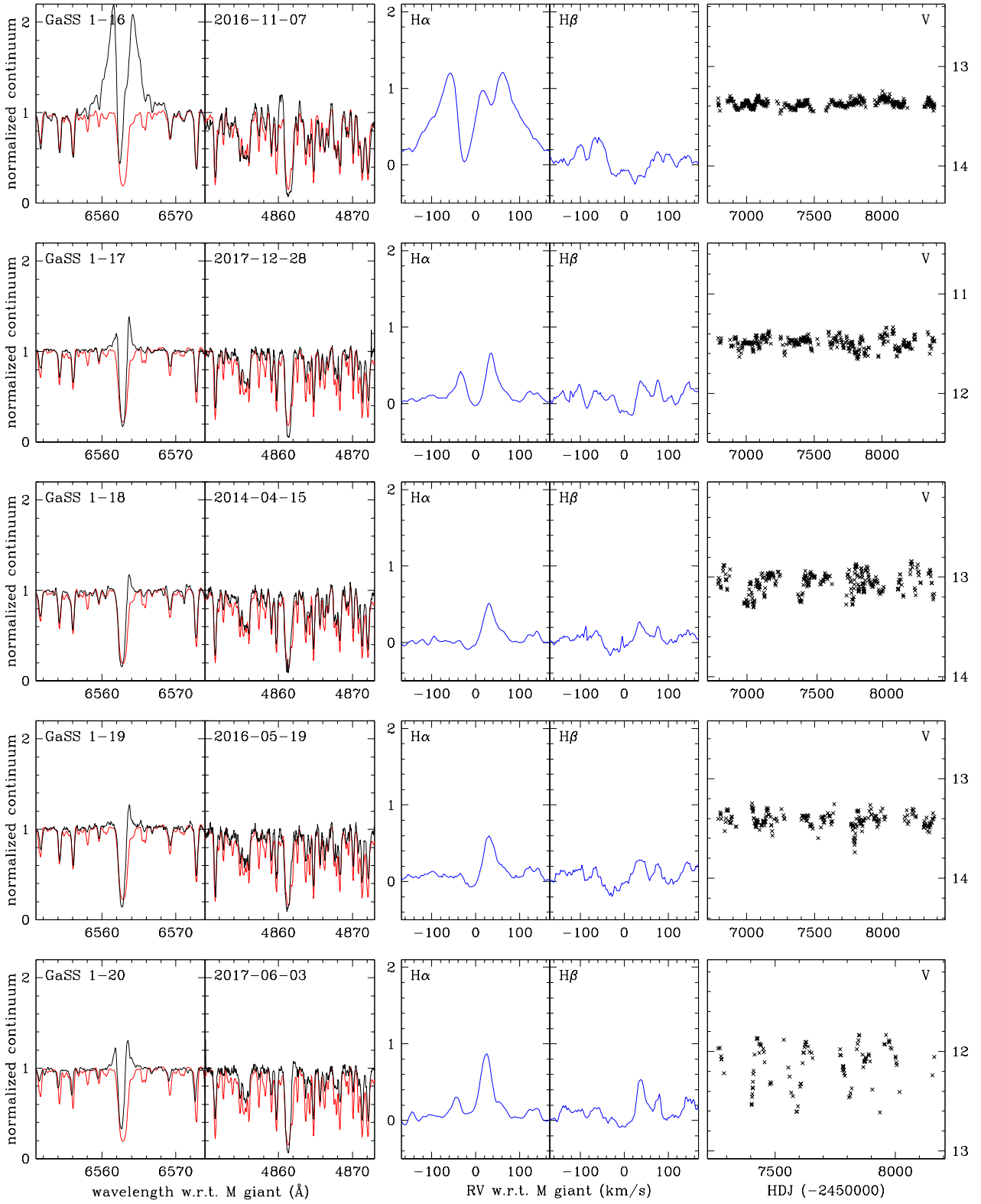


Figure A5. Similar to Fig. A2 for program stars GaSS 1-16 to GaSS 1-20.

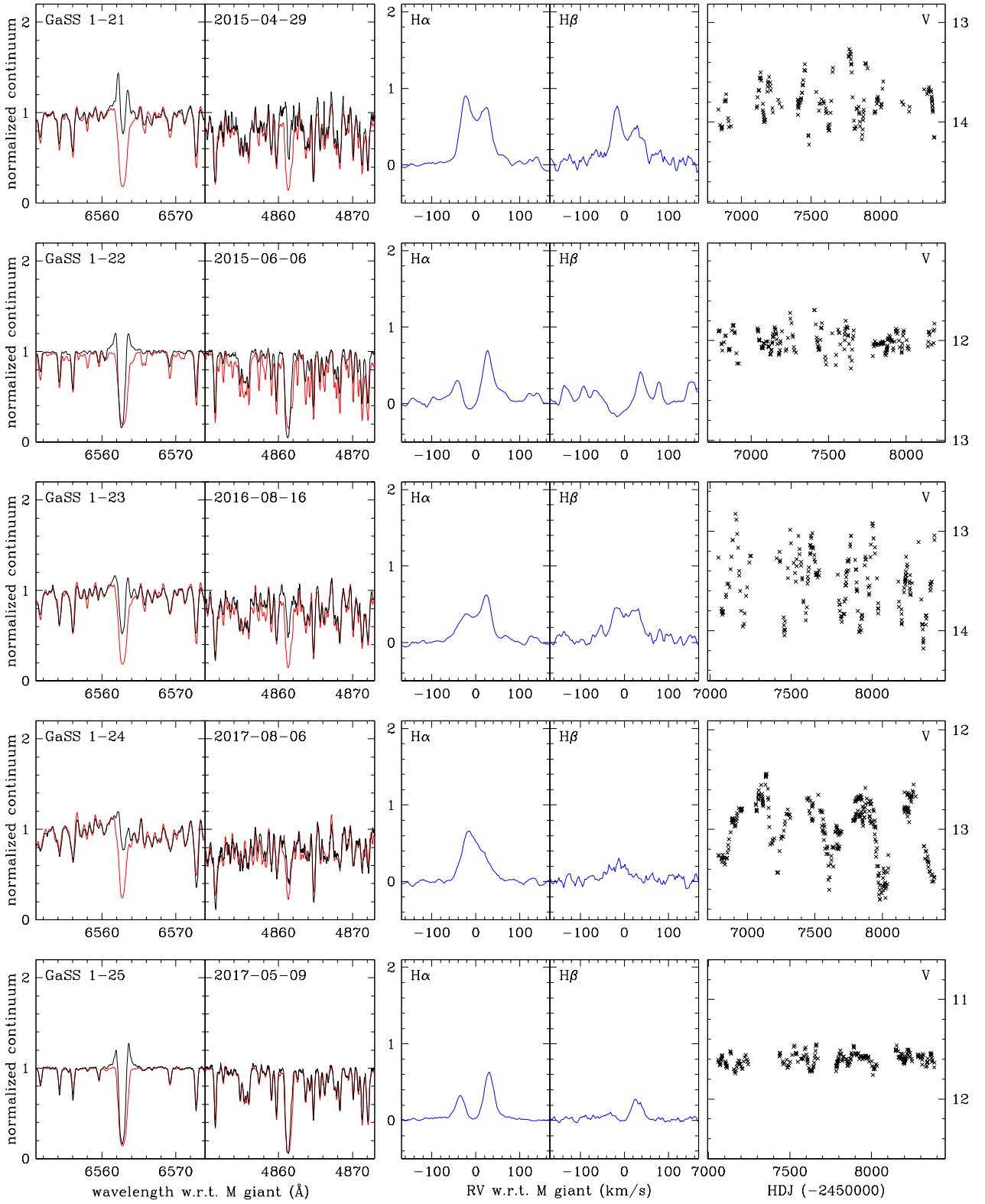


Figure A6. Similar to Fig. A2 for program stars GaSS 1-21 to GaSS 1-25.

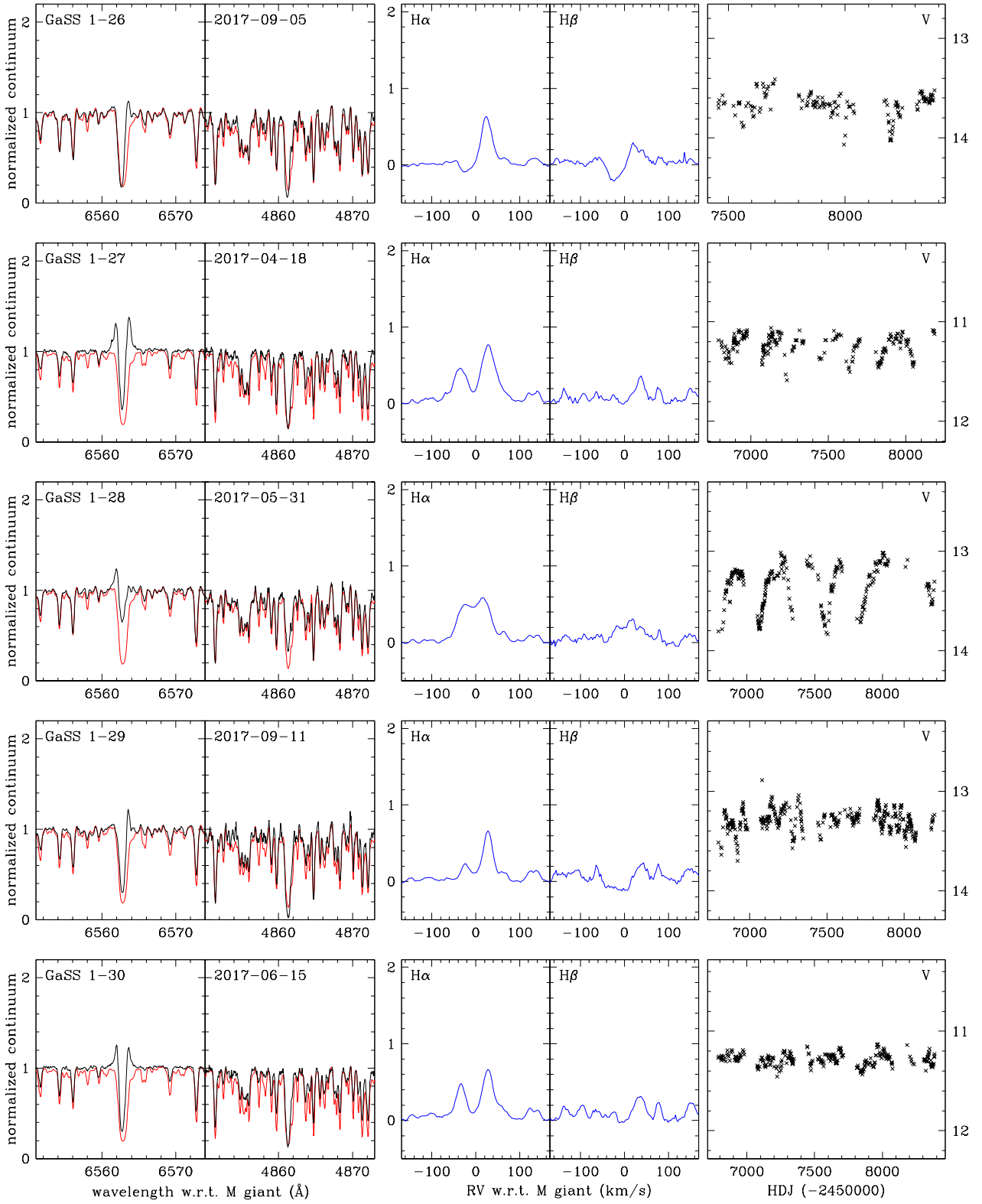


Figure A7. Similar to Fig. A2 for program stars GaSS 1-26 to GaSS 1-30.

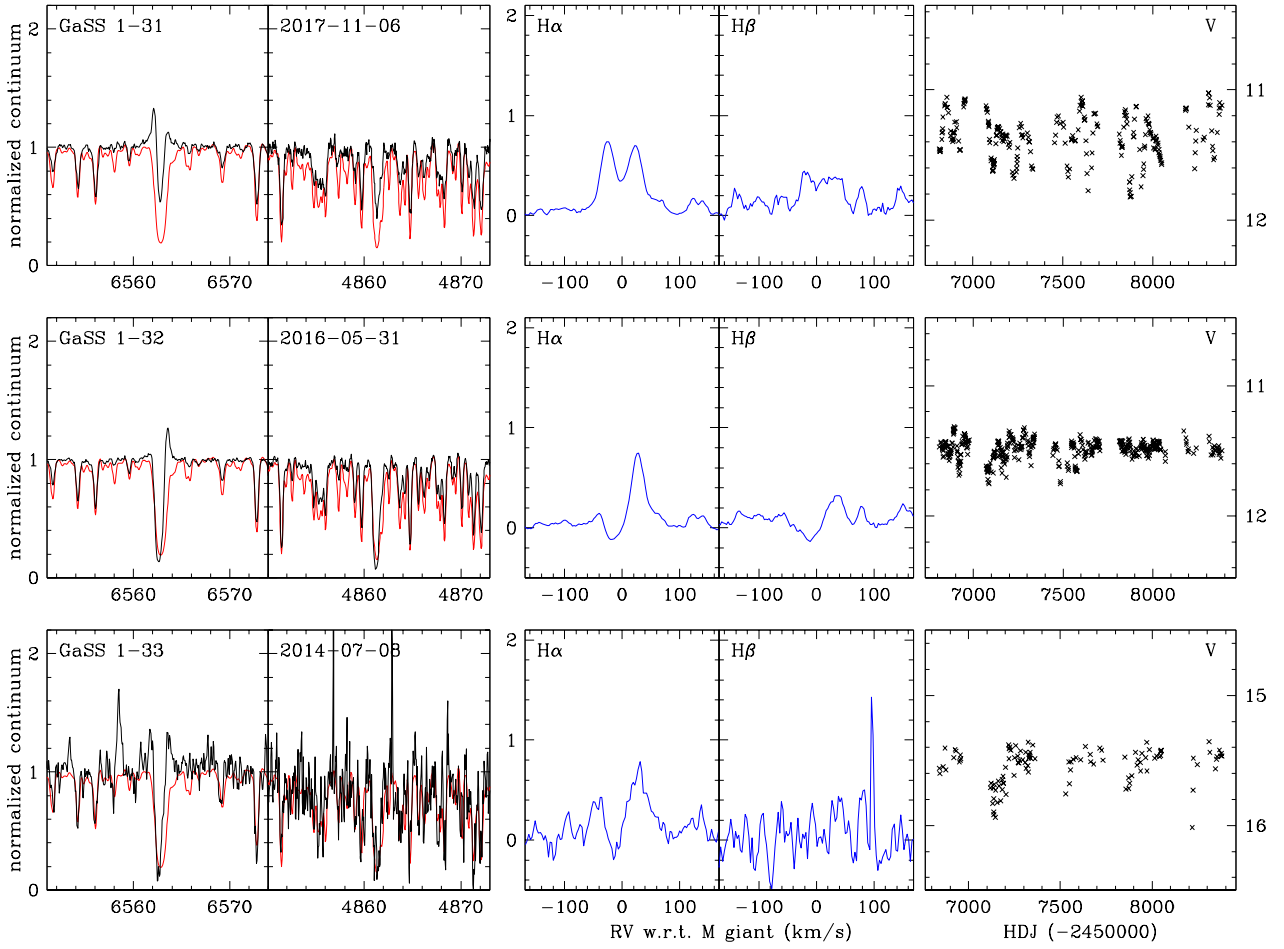


Figure A8. Similar to Fig. A2 for program stars GaSS 1-31 to GaSS 1-33.

This paper has been typeset from a $\text{\TeX}/\text{\LaTeX}$ file prepared by the author.

